

An Effective Model of the Retinoic Acid Induced HL-60 Differentiation Program

Ryan Tasseff, Holly A. Jensen, Johanna Congleton[†], Wei Dai, Katherine Rogers, Adithya Sagar, Rodica P. Bunaciu[†], Andrew Yen[†], and Jeffrey D. Varner*

Robert Frederick Smith School of Chemical and Biomolecular Engineering and [†]Department of Biomedical Sciences, Cornell University, Ithaca NY 14853

Running Title: Effective modeling of HL-60 differentiation

To be submitted: ?

*Corresponding author:

Jeffrey D. Varner,

Professor, Robert Frederick Smith School of Chemical and Biomolecular Engineering,
244 Olin Hall, Cornell University, Ithaca NY, 14853

Email: jdv27@cornell.edu

Phone: (607) 255 - 4258

Fax: (607) 255 - 9166

Abstract

In this study, we present an effective model All-Trans Retinoic Acid (ATRA)-induced differentiation of HL-60 cells. The model describes a key architectural feature of ATRA-induced differentiation, reinforcing feedback between an ATRA-inducible signalsome complex involving many proteins including Vav1, a guanine nucleotide exchange factor, and the activation of the mitogen activated protein kinase (MAPK) cascade. We decomposed the effective model into three modules; a signal initiation module that sensed and transformed an ATRA signal into program activation signals; a signal integration module that controlled the expression of upstream transcription factors; and a phenotype module which encoded the expression of functional differentiation markers from the ATRA-inducible transcription factors. The model, which was developed by integrating logical rules with kinetic modeling, was significantly smaller than previous models. However, despite its simplicity, it captured key features of ATRA induced differentiation of HL-60 cells. We identified an ensemble of effective model parameters using measurements taken from ATRA-induced HL-60 cells. Using these parameters, model analysis predicted that MAPK activation was bistable as a function of ATRA exposure. Conformational experiments supported ATRA-induced bistability. Additionally, the model captured intermediate and phenotypic gene expression data. Knockout analysis of the model suggested Gfi-1 and PPAR γ were critical to the ATRA-induced differentiation program. These findings, combined with other literature evidence, suggested that reinforcing feedback is central to a diversity of cell fate programs.

1 Introduction

2 Understanding the architecture of differentiation programs is an important therapeutic
3 challenge. Differentiation induction chemotherapy (DIC), using agents such as the vi-
4 tamin A derivative all-trans retinoic acid (ATRA), is a promising approach for the treat-
5 ment of many cancers (1–3). For example, ATRA treatment induces remission in 80–90%
6 of promyelocytic leukemia (APL) PML-RAR α -positive patients (4), thereby transforming
7 a fatal diagnosis into a manageable disease (5). However, remission is sometimes not
8 durable and relapsed cases exhibit emergent ATRA resistance (6, 7). To understand
9 the basis of this resistance, we must first understand the ATRA-induced differentiation
10 program. Toward this challenge, lessons learned in model systems, such as the lineage-
11 uncommitted human myeloblastic cell line HL-60 reported to closely resemble patient
12 derived cells (8), could inform our analysis of the differentiation programs occurring in
13 patients. Patient derived HL-60 leukemia cells have been a durable experimental model
14 since the 1970's to study differentiation (9). HL-60 undergoes cell cycle arrest and either
15 myeloid or monocytic differentiation following stimulation; ATRA induces G1/G0-arrest and
16 myeloid differentiation in HL-60 cells, while 1,25-dihydroxy vitamin D3 (D3) induces arrest
17 and monocytic differentiation. Commitment to cell cycle arrest and differentiation requires
18 approximately 48 hr of treatment, during which HL-60 cells undergo two division cycles.

19 Sustained mitogen-activated protein kinase (MAPK) activation is a defining feature of
20 ATRA-induced HL-60 differentiation. ATRA drives sustained activation of the Raf/MEK/ERK
21 pathway, leading to arrest and differentiation (10). Betraying a feedback loop, MEK inhi-
22 bition results in the loss of ERK and Raf phosphorylation, and the failure to arrest and
23 differentiate in response to ATRA (11). Retinoic acid (and its metabolites) are ligands
24 for the hormone activated nuclear transcription factors retinoic acid receptor (RAR) and
25 retinoid X receptor (RXR) (12). RAR/RXR activation is necessary for ATRA-induced Raf
26 phosphorylation (11), and the formation of an ATRA-inducible signalsome complex at the

membrane, which drives MAPK activation. While the makeup of the signalsome complex is not yet known, we do know that it is composed of Src family kinases Fgr and Lyn, PI3K, c-Cbl, Slp76, and KSR, plus transcription factors AhR and IRF1 (13–17). Signalsome activity is driven by ATRA-induced expression of CD38 and putatively the heterotrimeric Gq protein-coupled receptor BLR1 (18, 19). BLR1 (also known as CXCR5), identified as an early ATRA (or D3)-inducible gene using differential display (20), is necessary for MAPK activation and differentiation (19), and drives signalsome activity. Studies of the BLR1 promoter identified a non-canonical RARE site consisting of a 17 bp GT box approximately 1 kb upstream of the transcriptional start that conferred ATRA responsiveness (19). Members of the BLR1 transcriptional activator complex, e.g. NFATc3 and CREB, are phosphorylated by ERK, JNK or p38 MAPK family members suggesting positive feedback between the signalsome and MAPK activation (21). BLR1 overexpression enhanced Raf phosphorylation and accelerated terminal differentiation, while Raf inhibition reduced BLR1 expression and ATRA-induced terminal differentiation (22). In particular, Raf phosphorylation of the NFATc3 transcription factors at the BLR1 promoter enables transcriptional activation at the RARE by ATRA bound to RAR/RXR (23). BLR1 knock-out cells failed to activate Raf or differentiate in the presence of ATRA (22). Interestingly, both the knockdown or inhibition of Raf, also reduced BLR1 expression and functional differentiation (22). Thus, the expression of signalsome components e.g., BLR1 was Raf dependent, while Raf activation depended upon the signalsome. A previous computational study of ATRA-induced differentiation of HL-60 cells suggested that the BLR1-MAPK positive feedback circuit was sufficient to explain ATRA-induced sustained MAPK activation, and the expression of a limited number of functional differentiation markers (24). Model analysis also suggested that Raf was the most distinct of the MAPK proteins. However, this previous study developed and analyzed a complex model, thus leaving open the critical question of what is the minimal positive feedback circuit required to drive ATRA-induced

53 differentiation.

54 In this study, we explored this question using a minimal mathematical model of the
55 key architectural feature of ATRA induced differentiation of HL-60 cells, namely positive
56 feedback between an ATRA-inducible signalsome complex and MAPK activation. The
57 ATRA responsive signalsome-MAPK circuit was then used to drive a downstream gene
58 expression program which encoded for the expression of intermediate and functional dif-
59 ferentiation markers. The effective model used a novel framework which integrated logi-
60 cal rules with kinetic modeling to describe gene expression and protein regulation, while
61 largely relying upon biophysical parameters from the literature. This formulation signif-
62 icantly reduced the size and complexity of the model compared to the previous study
63 of Tasseff et al., while increasing the breadth of the biology described (24). The effec-
64 tive model, despite its simplicity, captured key features of ATRA induced differentiation of
65 HL-60 cells. Model analysis predicted the bistability of MAPK activation as a function of
66 ATRA exposure; conformational experiments supported ATRA-induced bistability. Model
67 simulations were also consistent with measurements of the influence of MAPK inhibitors,
68 and the failure of BLR1 knockout cells to differentiate when exposed to ATRA. In addition,
69 the expression of intermediate and phenotypic differentiation markers as also captured
70 following ATRA exposure. Lastly, we showed through immunoprecipitation and inhibitor
71 studies, that the guanine nucleotide exchange factor Vav1 is potentially a new ATRA-
72 inducible member of the signalsome complex functioning as a regulator that contributes
73 to signal amplification in the signalsome. Taken together, these findings when combined
74 with other literature evidence, suggested that positive feedback architectures are central
75 to differentiation programs generally, and necessary for ATRA-induced differentiation. The
76 model answers a biologically important question that is not easily experimentally attacked,
77 namely given the complexity of the signaling machine and the pathways it embodies, is
78 there a critical small suite of molecules that are the action elements seminal to eliciting

⁷⁹ ATRA-induced cell differentiation and G0 arrest.

80 **Results**

81 We constructed an effective model of ATRA-induced HL-60 differentiation which described
82 signaling and gene expression events following the addition of ATRA (Fig. 1). The model
83 connectivity was developed from literature and the studies presented here (Table 1). We
84 decomposed the ATRA program into three modules; a signal initiation module that sensed
85 and transformed the ATRA signal into activated cRaf-pS621 and the ATRA-RAR/RXR
86 (Trigger) signals (Fig. 1A); a signal integration module that controlled the expression of
87 upstream transcription factors given cRaf-pS621 and activated Trigger signals (Fig. 1B);
88 and a phenotype module which encoded the expression of functional differentiation mark-
89 ers from the ATRA-inducible transcription factors (Fig. 1C). Each component of these
90 modules was described by a mRNA and protein balance equation. Additionally, the sig-
91 nal initiation module also described the abundance of activated species e.g., Trigger and
92 cRaf-pS621 whose values were derived from unactivated Trigger and cRaf protein lev-
93 els. Lastly, because the population of HL-60 cells was dividing, we also considered a
94 dilution term in all balance equations. The signal initiation module contained nine dif-
95 ferential equations, while the signal integration and phenotype modules were collectively
96 encoded by 54 differential equations. Model parameters were taken from literature (Table
97 2), or estimated from experimental data using heuristic optimization (see materials and
98 methods).

99 The signal initiation module recapitulated sustained signalsome and MAPK activation
100 following exposure to $1\mu\text{M}$ ATRA (Fig. 2A-B). An ensemble of effective model param-
101 eters was estimated by minimizing the difference between simulations and time-series
102 measurements of BLR1 mRNA and cRaf-pS621 following the addition of $1\mu\text{M}$ ATRA. We
103 focused on the S621 phosphorylation site of cRaf since enhanced phosphorylation at this
104 site is a defining characteristic of sustained MAPK signaling activation in HL-60. The
105 effective model captured both ATRA-induced BLR1 expression (Fig. 2A) and sustained

106 phosphorylation of cRaf-pS621 (Fig. 2B) in a growing population of HL-60 cells. To-
107 gether, the reinforcing feedback within the signalsome and its embedded MAPK signaling
108 axis led to sustained activation over multiple cellular generations. However, the effective
109 model failed to capture the decline of BLR1 message after 48 hr of ATRA exposure. This
110 suggested that we captured the logic leading to the onset of differentiation, but failed to
111 describe program shutdown. Much of the focus in the literature has been on understand-
112 ing the initiation of differentiation, with little attention paid to understanding how a program
113 is terminated. This is a potential new direction that could be explored. Next, we tested
114 the response of the signal initiation module to different ATRA dosages.

115 The signal initiation model was bistable with respect to ATRA induction (Fig. 2C-D).
116 Phaseplane analysis predicted two stable steady-states when ATRA was present below
117 a critical threshold (Fig. 2C), and only a single steady-state above the threshold (Fig.
118 2D). In the lower stable state, neither the signalsome nor cRaf-pS621 were present (thus,
119 the differentiation program was inactive). However, at the higher stable state, both the
120 signalsome and cRaf-pS621 were present, allowing for sustained activation and differen-
121 tiation. Interestingly, when ATRA was above a critical threshold, only the activated state
122 was accessible (Fig. 2D). To test these findings, we first identified the ATRA threshold. We
123 exposed HL-60 cells to different ATRA concentrations for 72 hr (Fig. 2E). Morphological
124 changes associated with differentiation were visible for ATRA \geq 0.25 μ M, suggesting the
125 critical ATRA threshold was near this concentration. Next, we conducted ATRA washout
126 experiments to determine if activated cells remained activated in the absence of ATRA.
127 HL-60 cells locked into an activated state remained activated following ATRA withdraw-
128 (Fig. 3C). This sustained activation resulted from reinforcing feedback between the sig-
129 nalsome and the MAPK pathway. Thus, following activation, if we inhibited or removed
130 elements from the signal initiation module we expected the signalsome and MAPK signals
131 to decay. We simulated ATRA induced activation in the presence of kinase inhibitors, and

132 without key circuit elements. Consistent with experimental results using multiple MAPK
133 inhibitors, ATRA activation in the presence of MAPK inhibitors lowered the steady-state
134 value of signalsome (Fig. 3A). In the presence of BLR1, the signalsome and cRaf-pS621
135 signals were maintained following ATRA withdraw (Fig. 3B, gray). On the other hand,
136 BLR1 deletion removed the ability of the circuit to maintain a sustained MAPK response
137 following the withdraw of ATRA (Fig. 3B, blue). Lastly, washout experiments in which
138 cells were exposed to $1\mu\text{M}$ ATRA for 24 hr, and then transferred to fresh media with-
139 out ATRA, confirmed the persistence of the self sustaining activated state for up to 144
140 hr (Fig. 3C). Thus, these experiments confirmed that reinforcing positive feedback likely
141 drives the ATRA-induced differentiation program. Next, we analyzed the ATRA-induced
142 downstream gene expression program following signalsome and cRaf activation.

143 The signal integration and phenotype modules described ATRA-induced gene expres-
144 sion in wild-type HL-60 cells (Fig. 4). The signal initiation module produced two outputs,
145 activated Trigger and cRaf-pS621 which drove the expression of ATRA-induced transcrip-
146 tion factors, which then in turn activated the phenotypic program. In particular, Trigger (a
147 surrogate for the RAR α /RXR transcriptional complex) regulated the expression of the tran-
148 scription factors CCATT/enhancer binding protein α (C/EBP α), PU.1, and Egr-1. In turn,
149 these transcription factors, in combination with cRaf-pS621, regulated the expression of
150 downstream phenotypic markers such as CD38, CD11b or p47Phox. We assembled the
151 connectivity of the signal integration and phenotypic programs driven by Trigger and cRaf-
152 pS621 from literature (Table 1). We estimated the parameters for the signal initiation, and
153 phenotype modules from steady-state and dynamic measurements of transcription factor
154 and phenotypic marker expression following the addition of ATRA (25–28). However, the
155 bulk of the model parameters were taken from literature (29) and were not estimated in
156 this study (see materials and methods). The model simulations captured the time de-
157 pendent expression of CD38 and CD11b following the addition ATRA (Fig. 4A), and the

158 steady-state for signal integration and phenotypic markers (Fig. 4B). Lastly, we used the
159 *predicted* values of the p21 and E2F protein abundance to estimate a blackbox model of
160 ATRA-induced G0 arrest (Fig. 5). The phenotype module predicted p21 expression sig-
161 nificantly increased and E2F expression decreased, in response to ATRA exposure (Fig.
162 5A). We then used the ratio of these values in a polynomial model to calculate the frac-
163 tion of HL-60 cells in G0 arrest following the addition of ATRA (Fig. 5B). The third-order
164 polynomial model captured the trend in measured G0-arrest values as a function of time,
165 and was robust to uncertainty in the measured data (Fig. 5B, gray). Taken together, the
166 output of the signal integration and phenotypic modules was consistent with time-series
167 and steady-state measurements, thereby validating the assumed molecular connectivity.
168 Moreover, outputs from the phenotype module described the trend in ATRA-induced G0
169 cell cycle arrest. Next, we explored which nodes and interactions between nodes in the
170 signal integration module most influenced the system response.

171 The Gfi-1 and PPAR γ proteins were important regulators of ATRA-induced signal in-
172 tegration and phenotypic change (Fig. 6). We conducted pairwise gene knockout simula-
173 tions in the signal integration and phenotype modules to estimate which nodes controlled
174 the processing of the Trigger and cRaf-S621 signals. The difference between the sys-
175 tem state with and without the gene knockouts (encoded as a normalized state displace-
176 ment matrix) was decomposed using Singular Value Decomposition (SVD). A panel of
177 ten parameter sets was sampled, and the average normalized displacement matrix was
178 decomposed. The first six modes (approximately 36% of the total) described >95% of
179 the gene knockout variance, with the most important components of these modes being
180 the Gfi-1 and PPAR γ proteins, and to a lesser extent PU.1, C/EBP α and AP1 (Fig.
181 6A). To better understand which protein-DNA connections were important, we simulated
182 the pairwise deletion of interactions between these proteins and their respective regula-
183 tory targets. Singular value decomposition of the normalized state displacement matrix

assembled from the pairwise connection deletions, suggested the first six modes (approximately 26% of the total) accounted for >90% of the variance. Globally, the most sensitive interactions controlled p21 and p47Phox expression, markers for cell-cycle arrest and reactive oxygen formation phenotypic axes activated following ATRA addition (Fig. 6B). Analysis of the modes suggested the action of PPAR γ , Gfi-1 and C/EBP α were consistently important over multiple target genes. The connection knockout analysis also revealed robustness in the network. For example, no pair of deletions qualitatively changed the expression of regulators such as PU.1, Oct1, Oct4 or PPAR γ . Thus, the expression of these species was robust to disturbance in the connectivity. To better understand the combined influence of the PPAR γ and Gfi-1 deletions, we computed the fold change in the protein levels in the single (Gfi-1 $^{-/-}$ or PPAR γ $^{-/-}$) and double (Gfi-1 $^{-/-}$ and PPAR γ $^{-/-}$) mutants for the best fit parameter set (Fig. 7). Deletion of Gfi-1 led to a 2-4 fold increase in EGR-1, CD11b and C/EBP α expression, and a >8 fold increase in PU.1 abundance (Fig. 7, blue). On the other hand, deletion of PPAR γ led to >8 fold downregulation of CD38, p21, IRF1 and Oct1 (Fig. 7, red). Both knockouts slightly increased E2F expression, but neither influenced the expression of p47Phox. The double mutant was qualitatively similar to the combined behavior of the two single mutant cases. Taken together, Gfi-1 and PPAR γ controlled the cell-cycle arrest and receptor signaling axes, with PPAR γ regulating CD38, IRF1 and p21 expression while Gfi-1 controlled CD11b expression. These simulations suggested deletion of PPAR γ and Gfi-1 would not interfere with reactive oxygen formation, but would limit the ability of HL-60 cells to arrest. However, this analysis did not give insight into which components upstream of the signal initiation module were important. Toward this question, we explored the composition and regulation of the signalsome complex by experimentally interrogating a panel of possible Raf interaction partners.

The composition of the signalsome, and the kinase ultimately responsible for mediating ATRA-induced Raf activation is currently unknown. To explore this question, we

conducted immunoprecipitation and subsequent Western blotting to identify physical interactions between Raf and 19 putative interaction partners. A panel of 19 possible Raf interaction partners (kinases, GTPases, scaffolding proteins etc) was constructed based upon known signaling pathways. We did not consider the most likely binding partner, the small GTPase RAS, as previous studies have ruled it out in MAPK activation in HL-60 cells (22, 30). Total Raf was used as a bait protein for the immunoprecipitation studies. Interrogation of the Raf interactome suggested Vav1 was involved with ATRA-induced initiation of MAPK activity (Fig. 8). Western blot analysis using total Raf and Raf-pS621 specific antibodies confirmed the presence of the bait protein, total and phosphorylated forms, in the immunoprecipitate (Fig. 8A). Of the 19 proteins sampled, Vav1, Src, CK2, Akt, and 14-3-3 precipitated with Raf, suggesting a direct physical interaction was possible. However, only the associations between Raf and Vav1, and Raf and Src were ATRA-inducible (Fig. 8). Furthermore, the Vav1 and Src associations were correlated with Raf-pS621 abundance in the precipitate. Others proteins e.g., CK2, Akt and 14-3-3, generally bound Raf regardless of phosphorylation status or ATRA treatment. The remaining 14 proteins were expressed in whole cell lysate (Fig. 8B), but were not detectable in the precipitate of Raf IP. Treatment with the Raf kinase inhibitor GW5074 following ATRA exposure reduced the association of both Vav1 with Raf and Src with Raf (Fig. 8), although the signal intensity for Src was notably weak. However, GW5074 did not influence the association of CK2 or 14-3-3 with Raf, further demonstrating their independence from Raf phosphorylation. Interestingly, the Raf-Akt interaction qualitatively increased following treatment with GW5074; however, it remained unaffected by treatment with ATRA. Src family kinases are known to be important in myeloid differentiation (31) and their role in HL-60 differentiation has been investigated elsewhere (13). Given the existing work and variable reproducibility in the context of the Raf immunoprecipitate, we did not investigate the role of Src further in this study. Taken together, the immunoprecipitation and GW5074 results

236 implicated Vav1 association to be correlated with Raf activation following ATRA-treatment.
237 Previous studies demonstrated that a Vav1-Slp76-Cbl-CD38 complex plays an important
238 role in ATRA-induced MAPK activation and differentiation of HL-60 cells (15). Here we
239 did not observe direct interaction of Raf with Cbl or Slp76; however, this complex could
240 be involved upstream. Next, we considered the effect of the Raf kinase inhibitor GW5074
241 on functional markers of ATRA-induced growth arrest and differentiation.

242 Inhibition of Raf kinase activity modulated MAPK activation and differentiation mark-
243 ers following ATRA exposure (Fig. 8D-F). ATRA treatment alone statistically significantly
244 increased the G1/G0 percentage over the untreated control, while GW5074 alone had a
245 negligible effect on the cell cycle distribution (Fig. 8D). Surprisingly, the combination of
246 GW5074 and ATRA statistically significantly increased the G1/G0 population ($82 \pm 1\%$)
247 compared with ATRA alone ($61 \pm 0.5\%$). Increased G1/G0 arrest following the combined
248 treatment with GW5074 and ATRA was unexpected, as the combination of ATRA and the
249 MEK inhibitor (PD98059) has been shown previously to decrease ATRA-induced growth
250 arrest (10). However, growth arrest is not the sole indication of functional differentiation.
251 Expression of the cell surface marker CD11b has also been shown to coincide with HL-60
252 cells myeloid differentiation (32). We measured CD11b expression, for the various treat-
253 ment groups, using immuno-fluorescence flow cytometry 48 hr post-treatment. As with
254 G1/G0 arrest, ATRA alone increased CD11b expression over the untreated control, while
255 GW5074 further enhanced ATRA-induced CD11b expression (Fig. 8E). GW5074 alone
256 had no statistically significant effect on CD11b expression, compared with the untreated
257 control. Lastly, the inducible reactive oxygen species (ROS) response was used as a func-
258 tional marker of differentiated neutrophils (18). We measured the ROS response induced
259 by the phorbol ester 12-O-tetradecanoylphorbol-13-acetate (TPA) using flow cytometry.
260 Untreated cells showed no discernible TPA response, with only $7.0 \pm 3.0\%$ ROS induction
261 (Fig. 8F). Cells treated with ATRA had a significantly increased TPA response, $53 \pm 7\%$

²⁶² ROS induction 48 hr post-treatment. Treatment with both ATRA and GW5074 statistically
²⁶³ significantly reduced ROS induction ($22 \pm 0.6\%$) compared to ATRA alone. Interestingly,
²⁶⁴ Western blot analysis did not detect a GW5074 effect on ATRA-induced expression of
²⁶⁵ p47Phox, a required upstream component of the ROS response (Fig. 8F, bottom). Thus,
²⁶⁶ the inhibitory effect of GW5074 on inducible ROS might occur downstream of p47Phox
²⁶⁷ expression. However, the ROS producing complex is MAPK dependent, therefore it is
²⁶⁸ also possible that GW5074 inhibited ROS production by interfering with MAPK activation
²⁶⁹ (in which case the p47Phox marker might not accurately reflect phenotypic conversion
²⁷⁰ and differentiation).

271 **Discussion**

272 In this study, we presented an effective model of ATRA-inducible differentiation of HL-60
273 cells. The model consisted of three modules: a signal initiation module that sensed and
274 transformed the ATRA signal into activated cRaf-pS621 and the ATRA-RAR/RXR (Trig-
275 ger) signals; a signal integration module that controlled the expression of upstream tran-
276 scription factors given cRaf-pS621 and activated Trigger signals; and a phenotype mod-
277 ule which encoded the expression of functional differentiation markers from the ATRA-
278 inducible transcription factors. The model described the transcription and translation of
279 genes in each module, and signaling events in each module in a growing population of
280 HL-60 cells. Model parameters were taken from literature, however, unknown coefficients
281 that appear in the promoter logic models were estimated from protein measurements in
282 HL-60 cells following ATRA exposure. Despite its simplicity, the effective model captured
283 key features of the ATRA induced differentiation such as sustained MAPK activation, and
284 bistability with respect to ATRA exposure. The model also described the expression of
285 upstream transcription factors which regulated the expression of differentiation markers.
286 Lastly, analysis of the response of the model to perturbations identified Gfi-1 and PPAR γ
287 as master regulators of ATRA-induced differentiation. We also reported a new ATRA-
288 inducible component of the signalsome, Vav1. Vav1 is a guanine nucleotide exchange
289 factor for Rho family GTPases that activate pathways leading to actin cytoskeletal re-
290 arrangements and transcriptional alterations (33). The Vav1/Raf association correlated
291 with Raf activity, was ATRA-inducible and decreased after treatment with the Raf inhibitor
292 GW5074.

293 Naturally occurring cell fate decisions often incorporate reinforcing feedback and bista-
294 bility (34, 35). One of the most well studied cell fate circuits is the Mos mitogen-activated
295 protein kinase cascade in *Xenopus* oocytes. This cascade is activated when oocytes are
296 induced by the steroid hormone progesterone (36). The MEK-dependent activation of p42

297 MAPK stimulates the accumulation of the Mos oncoprotein, which in turn activates MEK,
298 thereby closing the feedback loop. This is similar to the signal initiation module presented
299 here; ATRA drives signalsome formation, which activates MAPK, which in turn leads to
300 more signalsome activation. Thus, while HL-60 and *Xenopus* oocytes are vastly different
301 biological models, their cell fate programs share a similar architectural feature. Reinforc-
302 ing feedback and bistability has also been implicated in hematopoietic cell fate determi-
303 nation. Laslo et al showed in nonmalignant myelomonocytic cells that the counter antag-
304 onistic repressors, Gfi-1 and Egr-1/2 (whose expression is tuned by PU.1 and C/EBP α),
305 encode a bistable switch that results in a macrophage, neutrophil or a mixed lineage pop-
306 ulation depending upon PU.1 and C/EBP α expression (35). The current model contained
307 the Gfi-1 and Egr-1/2 agonistic switch; however, its significance was unclear for HL-60
308 cells. The expression of Gfi-1, Egr-1/2, C/EBP α and PU.1 was not consistent with the
309 canonical lineage pattern expected from literature. For example, Egr-1/2 expression (as-
310 sociated with a macrophage lineage) increased, while Gfi-1 expression (associated with
311 a neutrophil lineage) remained constant following ATRA exposure. Thus, HL-60 cells,
312 which are a less mature cancer cell line, exhibited a non-canonical expression pattern.
313 Other unrelated cell fate decisions such as programmed cell death have also been sug-
314 gested to be bistable (37). Still more biochemical networks important to human health,
315 for example the human coagulation or complement cascades, also feature strong positive
316 feedback elements (38). Thus, while reinforcing feedback is often undesirable in human
317 engineered systems, it is at the core of a diverse variety of cell fate programs and other
318 networks important to human health.

319 Analysis of the signal integration and phenotype modules suggested that Gfi-1 and
320 PPAR γ were required for ATRA-induced differentiation in HL-60 cells. Model analysis
321 showed that PU.1, Egr-1 and C/EBP α expression increased in Gfi-1 $^{-/-}$ mutants, where
322 PU.1 expression was upregulated by greater than 8-fold. PU.1, a member of the *ets* tran-

scription factor family, is a well known regulator of granulocyte and monocyte development (39). The relative level of PU.1 and C/EBP α is thought to control macrophage versus neutrophil cell fate decisions in granulocytic macrophage progenitor cells (40). Simulations suggested that combined Gfi-1 + PPAR γ deletion crippled the ability of HL-60 cells to undergo neutrophilic differentiation following ATRA exposure. p21 expression decreased significantly, suggesting Gfi-1 $^{-/-}$ + PPAR γ $^{-/-}$ mutants were less likely to G0-arrest following ATRA exposure. The expression of other neutrophilic markers, such as CD38, also decreased in Gfi-1 $^{-/-}$ + PPAR γ $^{-/-}$ cells. On the other hand, the expression of reactive oxygen metabolic markers, or other important transcription factors such as Oct4 did not change. For example, model analysis suggested that the C/EBP α dependent interaction of PU.1 with the *NCF1* gene, which encodes the p47Phox protein, was the most sensitive PU.1 connection; deletion of this connection removed the ability of the system to express p47Phox. p47Phox, also known as neutrophil cytosol factor 1, is one of four cytosolic subunits of the multi-protein NADPH oxidase complex found in neutrophils (41). This enzyme is responsible for reactive oxygen species (ROS) production, a key component of the anti-microbial function of neutrophils. While p47Phox expression required C/EBP α and PU.1, neither Gfi-1 nor PPAR γ deletion increased expression. This suggested that p47Phox expression was saturated with respect to C/EBP α and PU.1, and simultaneously not sensitive to PPAR γ abundance. Taken together, Gfi-1 $^{-/-}$ + PPAR γ $^{-/-}$ cells were predicted to exhibit some aspects of the ATRA response, but not other critical features such as cell cycle arrest. Hock et al showed that Gfi-1 $^{-/-}$ mice lacked normal neutrophils, and were highly sensitive to bacterial infection (42). Thus, the model analysis was consistent with this study. However, other predictions concerning the behavior of the Gfi-1 $^{-/-}$ + PPAR γ $^{-/-}$ mutants have yet to be verified experimentally.

Immunoprecipitation studies identified a limited number of ATRA-dependent and - independent Raf interaction partners. While we were unable to detect the association

349 of Raf with common kinases and GTPases such as PKC, PKA, p38, Rac and Rho, we
350 did establish potential interactions between Raf and key partners such as Vav1, Src, Akt,
351 CK2 and 14-3-3. All of these partners are known to be associated with Raf activation
352 or function. Src is known to bind Raf through an SH2 domain, and this association has
353 been shown to be dependent of the serine phosphorylation of Raf (43). Thus, an ATRA in-
354 ductible Src/Raf association may be a result of ATRA-induced Raf phosphorylation at S259
355 or S621. We also identified an interaction between Raf and the Ser/Thr kinases Akt and
356 CK2. Akt can phosphorylate Raf at S259, as demonstrated by studies in a human breast
357 cancer line (44). CK2 can also phosphorylate Raf, although the literature has traditionally
358 focused on S338 and not S621 or S259(45). However, neither of these kinase interactions
359 were ATRA-inducible, suggesting their association with Raf alone was not associated with
360 ATRA-induced Raf phosphorylation. The adapter protein 14-3-3 was also constitutively
361 associated with Raf. The interaction between Raf and 14-3-3 has been associated with
362 both S621 and S259 phosphorylation and activity (46). Additionally, the association of
363 Raf with 14-3-3 not only stabilized S621 phosphorylation, but also reversed the S621
364 phosphorylation from inhibitory to activating (47). Finally, we found that Vav1/Raf associ-
365 ation correlated with Raf activity, was ATRA-inducible and decreased after treatment with
366 GW5074. The presence of Vav1 in Raf/Grb2 complexes has been shown to correlate with
367 increased Raf activity in mast cells (48). Furthermore, studies on Vav1 knockout mice
368 demonstrated that the loss of Vav1 resulted in deficiencies of ERK signaling for both T-
369 cells as well as neutrophils (49, 50). Interestingly, while an integrin ligand-induced ROS
370 response was blocked in Vav1 knockout neutrophils, TPA was able to bypass the Vav1
371 requirement and stimulate both ERK phosphorylation and ROS induction (50). In this
372 study, the TPA-induced ROS response was dependent upon Raf kinase activity, and was
373 mitigated by the addition of GW5074. It is possible that Vav1 is downstream of various
374 integrin receptors but upstream of Raf in terms of inducible ROS responses. Vav1 has

375 also been shown to associate with a Cbl-Slp76-CD38 complex in an ATRA-dependent
376 manner; furthermore, transfection of HL-60 cells with Cbl mutants that fail to bind CD38,
377 yet still bind Slp76 and Vav1, prevents ATRA-induced MAPK activation (15). The literature
378 suggest a variety of possible receptor-signaling pathways, which involve Vav1, for MAPK
379 activation; moreover, given the ATRA-inducible association Vav1 may play a direct role in
380 Raf activation.

381 We hypothesized that Vav1 is a member of an ATRA-inducible complex which propels
382 sustained MAPK activation, arrest and differentiation. Initially, ATRA-induced Vav1 ex-
383 pression drives increased association between Vav1 and Raf. This increased interaction
384 facilitates phosphorylation and activation of Raf by pre-bound Akt and/or CK2 at S621
385 or perhaps S259. Constitutively bound 14-3-3 may also stabilize the S621 phosphory-
386 lation, modulate the activity and/or up-regulate autophosphorylation. Activated Raf can
387 then drive ERK activation, which in turn closes the positive feedback loop by activating
388 Raf transcription factors e.g., Sp1 and/or STAT1 (51–54). We tested this working hy-
389 pothesis using mathematical modeling. The model recapitulated both ATRA time-course
390 data as well as the GW5074 inhibitor effects. This suggested the proposed Raf-Vav1
391 architecture was at least consistent with the experimental studies. Further, analysis of
392 the Raf-Vav1 model identified bistability in ppERK levels. Thus, two possible MAPK ac-
393 tivation branches were possible for experimentally testable ATRA values. The analysis
394 also suggested the ATRA-induced Raf-Vav1 architecture could be locked into a sustained
395 signaling mode (high ppERK) even in the absence of a ATRA signal. This locked-in prop-
396 erty could give rise to an ATRA-induction memory. We validated the treatment memory
397 property predicted by the Raf-Vav1 circuit experimentally using ATRA-washout experi-
398 ments. ERK phosphorylation levels remained high for more than 96 hr after ATRA was
399 removed. Previous studies demonstrated that HL-60 cells possessed an inheritable mem-
400 ory of ATRA stimulus (55). Although the active state was self-sustaining, the inactive state

401 demonstrated considerable robustness to perturbation. For example, we found that 50x
402 overexpression of Raf was required to reliably lock MAPK into the activated state, while
403 small perturbations had almost no effect on ppERK levels over the entire ensemble. CD38
404 expression correlated with the ppERK, suggesting its involvement in the signaling com-
405 plex. Our computational and experimental results showed that positive feedback, through
406 ERK-dependent Raf expression, could sustain MAPK signaling through many division cy-
407 cles. Such molecular mechanisms could underly aspects of cellular memory associated
408 to consecutive ATRA treatments.

409 **Materials and Methods**

410 *Effective gene expression model equations.* We decomposed the ATRA-induced differ-
 411 entiation program into three modules; a signal initiation module that sensed and trans-
 412 formed the ATRA signal into activated cRaf-pS621 and the ATRA-RAR/RXR (activated
 413 Trigger) signals; a signal integration module that controlled the expression of upstream
 414 transcription factors given cRaf-pS621 and activated Trigger signals; and a phenotype
 415 module which encoded the expression of functional differentiation markers from the ATRA-
 416 inducible transcription factors. The output of the signal initiation module was the input to
 417 the gene expression model. For each gene $j = 1, 2, \dots, \mathcal{G}$, we modeled both the mRNA
 418 (m_j), protein (p_j) and signaling species abundance:

$$\frac{dm_j}{dt} = r_{T,j} - (\mu + \theta_{m,j}) m_j + \lambda_j \quad (1)$$

$$\frac{dp_j}{dt} = r_{X,j} - (\mu + \theta_{p,j}) p_j \quad (2)$$

$$g(p_1, \dots, p_{\mathcal{G}}, \kappa) = 0 \quad (3)$$

419 The terms $r_{T,j}$ and $r_{X,j}$ denote the specific rates of transcription, and translation while
 420 the terms $\theta_{m,j}$ and $\theta_{p,j}$ denote first-order degradation constants for mRNA and protein,
 421 respectively. The specific transcription rate $r_{T,j}$ was modeled as the product of a kinetic
 422 term $\bar{r}_{T,j}$ and a control term u_j which described how the abundance of transcription fac-
 423 tors, or other regulators influenced the expression of gene j . The kinetic transcription
 424 term $\bar{r}_{T,j}$ was modeled as:

$$\bar{r}_{T,j} = V_T^{max} \left(\frac{L_{T,o}}{L_{T,j}} \right) \left(\frac{G_j}{K_T + G_j} \right) \quad (4)$$

425 where the maximum gene expression rate V_T^{max} was defined as the product of a char-
 426 acteristic transcription rate constant (k_T) and the abundance of RNA polymerase (R_1),

427 $V_T^{max} = k_T(R_1)$. The $(L_{T,o}/L_{T,j})$ term denotes the ratio of transcription read lengths; $L_{T,o}$
 428 represents a characteristic gene length, while $L_{T,j}$ denotes the length of gene j . Thus, the
 429 ratio $(L_{T,o}/L_{T,j})$ is a gene specific correction to the characteristic transcription rate V_T^{max} .
 430 Lastly, the λ_j term denotes the constitutive rate of expression of gene j .

431 The gene expression control term $0 \leq u_j \leq 1$ depended upon the combination of fac-
 432 tors which influenced the expression of gene j . If the expression of gene j was influenced
 433 by $1, \dots, m$ factors, we modeled this relationship as $u_j = \mathcal{I}_j(f_{1j}(\cdot), \dots, f_{mj}(\cdot))$ where
 434 $0 \leq f_{ij}(\cdot) \leq 1$ denotes a regulatory transfer function quantifying the influence of factor i
 435 on the expression of gene j , and $\mathcal{I}_j(\cdot)$ denotes an integration rule which combines the
 436 individual regulatory inputs for gene j into a single control term. In this study, the integra-
 437 tion rule governing gene expression was the weighted fraction of promoter configurations
 438 that resulted in gene expression (56):

$$u_j = \frac{W_{R_{1,j}} + \sum_n W_{nj} f_{nj}}{1 + W_{R_{1,j}} + \sum_d W_{dj} f_{dj}} \quad (5)$$

439 The numerator, the weighted sum (with weights W_{nj}) of promoter configurations leading to
 440 gene expression, was normalized by all possible promoter configurations. The likelihood
 441 of each configuration was quantified by the transfer function f_{nj} (which we modeled using
 442 Hill like functions), while the lead term in the numerator $W_{R_{1,j}}$ denotes the weight of con-
 443 stitutive expression for gene j . Given this formulation, the rate of constitutive expression
 444 was then given by:

$$\lambda_j = \bar{r}_{T,j} \left(\frac{W_{R_{1,j}}}{1 + W_{R_{1,j}}} \right) \quad (6)$$

445 If a gene expression process had no modifying factors, $u_j = 1$. Lastly, the specific trans-

446 lation rate was modeled as:

$$r_{X,j} = V_X^{max} \left(\frac{L_{X,o}}{L_{X,j}} \right) \left(\frac{m_j}{K_X + m_j} \right) \quad (7)$$

447 where V_X^{max} denotes a characteristic maximum translation rate estimated from literature,
448 and K_X denotes a translation saturation constant. The characteristic maximum translation
449 rate was defined as the product of a characteristic translation rate constant (k_X) and
450 the Ribosome abundance (R_2), $V_X^{max} = k_X (R_2)$. As was the case for transcription, we
451 corrected the characteristic translation rate by the ratio of the length of a characteristic
452 transcription normalized by the length of transcript j .

453 *Signaling model equations.* The signal initiation, and integration modules required the
454 abundance of cRaf-pS621 and ATRA-RAR/RXR (activated Trigger) as inputs. However,
455 our base model described only the abundance of inactive proteins e.g., cRaf or RXR/RAR
456 but not the activated forms. To address this issue, we estimated pseudo steady state
457 approximations for the abundance of cRaf-pS621 and activated Trigger. The abundance
458 of activated trigger ($x_{a,1}$) was estimated directly from the RXR/RAR abundance ($x_{u,1}$):

$$x_{a,1} \sim x_{u,1} \left(\frac{\alpha \cdot \text{ATRA}}{1 + \alpha \cdot \text{ATRA}} \right) \quad (8)$$

459 where α denotes a gain parameter; $\alpha = 0.0$ if ATRA is less than a threshold, and $\alpha = 0.1$
460 if ATRA is greater than the differentiation threshold. The abundance of cRaf-pS621 was
461 estimated by making the pseudo steady state approximation on the cRaf-pS621 balance.
462 The abundance of an activated signaling species i was given by:

$$\frac{dx_i}{dt} = r_{+,i}(\mathbf{x}, \mathbf{k}) - (\mu + k_{d,i}) x_i \quad i = 1, \dots, \mathcal{M} \quad (9)$$

463 The quantity x_i denotes concentration of signaling species i , while \mathcal{R} and \mathcal{M} denote
 464 the number of signaling reactions and signaling species in the model, respectively. The
 465 term $r_{+,i}(\mathbf{x}, \mathbf{k})$ denotes the rate of generation of activated species i , while μ denotes
 466 the specific growth rate, and $k_{d,i}$ denotes the rate constant controlling the non-specific
 467 degradation of x_i . We neglected deactivation reactions e.g., phosphatase activities. We
 468 assumed that signaling processes were fast compared to gene expression; this allowed
 469 us to approximate the signaling balance as:

$$x_i^* \simeq \frac{r_{+,i}(\mathbf{x}, \mathbf{k})}{(\mu + k_{d,i})} \quad i = 1, \dots, \mathcal{M} \quad (10)$$

470 The generation rate was written as the product of a kinetic term ($\bar{r}_{+,i}$) and a control term
 471 (v_i). The control terms $0 \leq v_j \leq 1$ depended upon the combination of factors which in-
 472 fluenced rate process j . If rate j was influenced by $1, \dots, m$ factors, we modeled this
 473 relationship as $v_j = \mathcal{I}_j(f_{1j}(\cdot), \dots, f_{mj}(\cdot))$ where $0 \leq f_{ij}(\cdot) \leq 1$ denotes a regulatory
 474 transfer function quantifying the influence of factor i on rate j . The function $\mathcal{I}_j(\cdot)$ is an
 475 integration rule which maps the output of regulatory transfer functions into a control vari-
 476 able. In this study, we used $\mathcal{I}_j \in \{\min, \max\}$ and hill transfer functions (57). If a process
 477 had no modifying factors, $v_j = 1$. The kinetic rate of cRaf-pS621 generation $\bar{r}_{+,cRaf}$ was
 478 modeled as:

$$\bar{r}_{+,cRaf} = k_{+,cRaf} x_s \left(\frac{x_{cRaf}}{K_{+,cRaf} + x_{cRaf}} \right) \quad (11)$$

479 where x_s denotes the signalsome abundance, and $K_{+,cRaf}$ denotes a saturation constant
 480 governing cRaf-pS621 formation. The formation of cRaf-pS621 was regulated by only a
 481 single factor, the abundance of MAPK inhibitor, thus $v_{+,cRaf}$ took the form:

$$v_{+,cRaf} = \left(1 - \frac{I}{K_D + I} \right) \quad (12)$$

482 where I denotes the abundance of the MAPK inhibitor, and K_D denotes the inhibitor
483 affinity.

484 *Estimation of gene expression model parameters.* We estimated parameters appearing
485 in the mRNA and protein balances, the abundance of polymerases and ribosomes, tran-
486 scription and translation rates, the half-life of a typical mRNA and protein, and typical
487 values for the copies per cell of RNA polymerase and ribosomes from literature (Table 2).
488 The saturation constants K_X and K_T were adjusted so that gene expression and trans-
489 lation resulted in gene products on a biologically realistic concentration scale. Lastly, we
490 calculated the concentration for gene G_j by assuming, on average, that a cell had two
491 copies of each gene at any given time. Thus, the bulk of our gene expression model pa-
492 rameters were based directly upon literature values, and were not adjusted during model
493 identification. However, the remaining parameters, e.g., the W_{ij} appearing in the gene
494 expression control laws, or parameters appearing in the transfer functions f_{dij} , were esti-
495 mated from the protein expression and signaling data sets discussed here.

496 Signaling and gene expression model parameters were estimated by minimizing the
497 squared difference between simulations and experimental protein data set j . We mea-
498 sured the squared difference in the scale, fold change and shape for protein j :

$$E_j(\mathbf{k}) = \left(\mathcal{M}_j(t_-) - \hat{y}_j(t_-, \mathbf{k}) \right)^2 + \sum_{i=1}^{\mathcal{T}_j} \left(\hat{\mathcal{M}}_{ij} - \hat{y}_{ij}(\mathbf{k}) \right)^2 + \sum_{i=1}^{\mathcal{T}_j} \left(\mathcal{M}'_{ij} - y'_{ij}(\mathbf{k}) \right)^2 \quad (13)$$

499 The first term in Eq. (13) quantified the initial *scale* error, directly before the addition
500 of ATRA. In this case, $\mathcal{M}_j(t_-)$ (the approximate concentration of protein j before the
501 addition of ATRA) was estimated from literature. This term was required because the
502 protein measurements were reported as the fold-change; thus, the data was normalized
503 by a control value measured before the addition of ATRA. However, the model operated on
504 a physical scale. The first term allowed the model to capture physically realistic changes

following ATRA addition. The second term quantified the difference in the *fold-change* of protein j as a function of time. The terms $\hat{\mathcal{M}}_{ij}$ and \hat{y}_{ij} denote the scaled experimental observations and simulation outputs (fold-change; protein normalized by control value directly before ATRA addition) at time i from protein j , where T_j denoted the number of time points for data set j . Lastly, the third term of the objective function measured the difference in the *shape* of the measured and simulated protein levels. The scaled value $0 \leq \mathcal{M}'_{ij} \leq 1$ was given by:

$$\hat{\mathcal{M}}_{ij} = \left(\mathcal{M}_{ij} - \min_i \mathcal{M}_{ij} \right) / \left(\max_i \mathcal{M}_{ij} - \min_i \mathcal{M}_{ij} \right) \quad (14)$$

where $\mathcal{M}'_{ij} = 0$ and $\mathcal{M}'_{ij} = 1$ describe the lowest (highest) intensity bands. A similar scaling was used for the simulation output. We minimized the total model residual $\sum_j E_j$ using a heuristic direct-search optimization procedure, subject to box constraints on the parameter values, starting from a random initial parameter guess. Each downhill step was archived and used for ensemble calculations. The optimization procedure (a covariance matrix adaptation evolution strategy) has been reported previously (58).

Estimation of an effective cell cycle arrest model. We formulated an effective N-order polynomial model of the fraction of cells undergoing ATRA-induced cell cycle arrest at time t , $\hat{\mathcal{A}}(t)$, as:

$$\hat{\mathcal{A}}(t) \simeq a_0 + \sum_{i=1}^{N-1} a_i \phi_i(\mathbf{p}(t), t) \quad (15)$$

where a_i were unknown parameters, and $\phi_i(\mathbf{p}(t), t)$ denotes a basis function. The basis functions were dependent upon the system state; in this study, we assumed $N = 4$ and basis functions of the form:

$$\phi_i(\mathbf{p}(t), t) = \left(\frac{t}{T} + \frac{p21}{E2F} \Big|_t \right)^{(i-1)} \quad (16)$$

524 The parameters a_0, \dots, a_3 were estimated directly from cell-cycle measurements (biologi-
525 cal replicates) using least-squares.

526 *Availability of model code.* The signaling and gene expression model equations, and the
527 parameter estimation procedure, were implemented in the Julia programming language.
528 The model equations were solved using the ODE23s routine of the ODE package (59). The
529 model code and parameter ensemble is freely available under an MIT software license
530 and can be downloaded from <http://www.varnerlab.org>.

531 *Cell culture and treatment* Human myeloblastic leukemia cells (HL-60 cells) were grown
532 in a humidified atmosphere of 5% CO₂ at 37°C and maintained in RPMI 1640 from Gibco
533 (Carlsbad, CA) supplemented with 5% heat inactivated fetal bovine serum from Hyclone
534 (Logan, UT) and 1× antibiotic/antimicotic (Gibco, Carlsbad, CA). Cells were cultured in
535 constant exponential growth (60). Experimental cultures were initiated at 0.1×10^6 cells/mL
536 24 hr prior to ATRA treatment; if indicated, cells were also treated with GW5074 (2 μ M) 18
537 hr before ATRA treatment. For the cell culture washout experiments, cells were treated
538 with ATRA for 24 hr, washed 3x with prewarmed serum supplemented culture medium
539 to remove ATRA, and reseeded in ATRA-free media as described. Western blot analysis
540 was performed at incremental time points after removal of ATRA.

541 *Chemicals* All-Trans Retinoic Acid (ATRA) from Sigma-Aldrich (St. Louis, MO) was dis-
542 solved in 100% ethanol with a stock concentration of 5mM, and used at a final concen-
543 tration of 1 μ M (unless otherwise noted). The cRaf inhibitor GW5074 from Sigma-Aldrich
544 (St. Louis, MO) was dissolved in DMSO with a stock concentration of 10mM, and used
545 at a final concentration of 2 μ M. HL-60 cells were treated with 2 μ M GW5074 with or with-
546 out ATRA (1 μ M) at 0 hr. This GW5074 dosage had a negligible effect on the cell cycle
547 distribution, compared to ATRA treatment alone.

548 *Immunoprecipitation and western blotting* Approximately 1.2×10^7 cells were lysed using
549 $400\mu\text{L}$ of M-Per lysis buffer from Thermo Scientific (Waltham, MA). Lysates were cleared
550 by centrifugation at $16,950 \times g$ in a micro-centrifuge for 20 min at 4°C . Lysates were
551 pre-cleared using $100\mu\text{L}$ protein A/G Plus agarose beads from Santa Cruz Biotechnology
552 (Santa Cruz, CA) by inverting overnight at 4°C . Beads were cleared by centrifugation and
553 total protein concentration was determined by a BCA assay (Thermo Scientific, Waltham,
554 MA). Immunoprecipitations were setup by bringing lysate to a concentration of 1g/L in a
555 total volume of $300\mu\text{L}$ (M-Per buffer was used for dilution). The anti-Raf antibody was
556 added at $3\mu\text{L}$. A negative control with no bait protein was also used to exclude the di-
557 rect interaction of proteins with the A/G beads. After 1 hr of inversion at 4°C , $20\mu\text{L}$ of
558 agarose beads was added and samples were left to invert overnight at 4°C . Samples
559 were then washed three times with M-Per buffer by centrifugation. Finally proteins were
560 eluted from agarose beads using a laemmli loading buffer. Eluted proteins were resolved
561 by SDS-PAGE and Western blotting. Total lysate samples were normalized by total protein
562 concentration ($20\mu\text{g}$ per sample) and resolved by SDS-PAGE and Western blotting. Sec-
563 ondary HRP bound antibody was used for visualization. All antibodies were purchased
564 from Cell Signaling (Boston, MA) with the exception of α -p621 Raf which was purchased
565 from Biosource/Invitrogen (Carlsbad, CA), and α -CK2 from BD Biosciences (San Jose,
566 CA).

567 *Morphology assessment* Untreated and ATRA-treated HL-60 cells were collected after
568 72 hr and cytocentrifuged for 3 min at 700 rpm onto glass slides. Slides were air-dried
569 and stained with Wright's stain. Slide images were captured at 40X (Leica DM LB 100T
570 microscope, Leica Microsystems).

571 **Competing interests**

572 The authors declare that they have no competing interests.

573 **Author's contributions**

574 J.V and A.Y directed the study. R.T, H.J, R.B and J.C conducted the cell culture measure-
575 ments. J.V, R.B, W.D, K.R and A.S developed the reduced order HL-60 models and the
576 parameter ensemble. W.D and J.V analyzed the model ensemble, and generated figures
577 for the manuscript. The manuscript was prepared and edited for publication by W.D, R.B,
578 A.Y and J.V.

579 **Acknowledgements**

580 We gratefully acknowledge the suggestions from the anonymous reviewers to improve
581 this manuscript.

582 **Funding**

583 We acknowledge the financial support to J.V. by the National Science Foundation CA-
584 REER (CBET-0846876) for the support of R.T. and H.J. In addition, we acknowledge
585 support to A.Y. from the National Institutes of Health (CA 30555, CA152870) and a grant
586 from New York State Stem Cell Science. Lastly, we acknowledge the financial support to
587 J.V. and A.Y. from the National Cancer Institute (#U54 CA143876). The content is solely
588 the responsibility of the authors and does not necessarily represent the official views of
589 the National Cancer Institute or the National Institutes of Health.

590 **References**

- 591 1. Bushue N, Wan YJY (2010) Retinoid pathway and cancer therapeutics. *Adv Drug*
592 *Deliv Rev* 62: 1285-98.
- 593 2. Tang XH, Gudas LJ (2011) Retinoids, retinoic acid receptors, and cancer. *Annu Rev*
594 *Pathol* 6: 345-64.
- 595 3. Cheung FSG, Lovicu FJ, Reichardt JKV (2012) Current progress in using vitamin d
596 and its analogs for cancer prevention and treatment. *Expert Rev Anticancer Ther*
597 12: 811-37.
- 598 4. Nilsson B (1984) Probable in vivo induction of differentiation by retinoic acid of
599 promyelocytes in acute promyelocytic leukaemia. *Br J Haematol* 57: 365-71.
- 600 5. Coombs CC, Tavakkoli M, Tallman MS (2015) Acute promyelocytic leukemia: where
601 did we start, where are we now, and the future. *Blood Cancer J* 5: e304.
- 602 6. Warrell RP Jr (1993) Retinoid resistance in acute promyelocytic leukemia: new
603 mechanisms, strategies, and implications. *Blood* 82: 1949-53.
- 604 7. Freemantle SJ, Spinella MJ, Dmitrovsky E (2003) Retinoids in cancer therapy and
605 chemoprevention: promise meets resistance. *Oncogene* 22: 7305-15.
- 606 8. Harrison JS, Wang X, Studzinski GP (2016) The role of vdr and bim in potentiation
607 of cytarabine-induced cell death in human aml blasts. *Oncotarget* 7: 36447-36460.
- 608 9. Breitman TR, Selonick SE, Collins SJ (1980) Induction of differentiation of the hu-
609 man promyelocytic leukemia cell line (HL-60) by retinoic acid. *Proc Natl Acad Sci U*
610 *S A* 77: 2936–2940.
- 611 10. Yen A, Roberson MS, Varvayanis S, Lee AT (1998) Retinoic acid induced
612 mitogen-activated protein (MAP)/extracellular signal-regulated kinase (ERK) kinase-
613 dependent MAP kinase activation needed to elicit HL-60 cell differentiation and
614 growth arrest. *Cancer Res* 58: 3163–3172.
- 615 11. Hong HY, Varvayanis S, Yen A (2001) Retinoic acid causes MEK-dependent RAF

- 616 phosphorylation through RARalpha plus RXR activation in HL-60 cells. Differentiation 68: 55–66.
- 617
- 618 12. Mangelsdorf DJ, Ong ES, Dyck JA, Evans RM (1990) Nuclear receptor that identifies
- 619 a novel retinoic acid response pathway. Nature 345: 224–229.
- 620 13. Congleton J, MacDonald R, Yen A (2012) Src inhibitors, PP2 and dasatinib, increase
- 621 retinoic acid-induced association of Lyn and c-Raf (S259) and enhance MAPK-
- 622 dependent differentiation of myeloid leukemia cells. Leukemia 26: 1180-8.
- 623 14. Shen M, Bunaci R, Congleton J, Jensen H, Sayam L, et al. (2011) Interferon regu-
- 624 latory factor-1 binds c-Cbl, enhances mitogen activated protein kinase signaling and
- 625 promotes retinoic acid-induced differentiation of HL-60 human myelo-monoblastic
- 626 leukemia cells. Leuk Lymphoma 52: 2372-9.
- 627 15. Shen M, Yen A (2009) c-Cbl tyrosine kinase-binding domain mutant G306E abol-
- 628 ishes the interaction of c-Cbl with CD38 and fails to promote retinoic acid-induced
- 629 cell differentiation and G0 arrest. J Biol Chem 284: 25664–25677.
- 630 16. Yen A, Varvayanis S, Smith J, Lamkin T (2006) Retinoic acid induces expression of
- 631 SLP-76: expression with c-FMS enhances ERK activation and retinoic acid-induced
- 632 differentiation/G0 arrest of HL-60 cells. Eur J Cell Biol 85: 117–132.
- 633 17. Marchisio M, Bertagnolo V, Colamussi ML, Capitani S, Neri LM (1998) Phos-
- 634 phatidylinositol 3-kinase in HL-60 nuclei is bound to the nuclear matrix and increases
- 635 during granulocytic differentiation. Biochem Biophys Res Commun 253: 346-51.
- 636 18. Congleton J, Jiang H, Malavasi F, Lin H, Yen A (2011) ATRA-induced HL-60 myeloid
- 637 leukemia cell differentiation depends on the CD38 cytosolic tail needed for mem-
- 638 brane localization, but CD38 enzymatic activity is unnecessary. Exp Cell Res 317:
- 639 910–919.
- 640 19. Wang J, Yen A (2004) A novel retinoic acid-responsive element regulates retinoic
- 641 acid induced BLR1 expression. Mol Cell Biol 24: 2423 - 2443.

- 642 20. Yen A (1990) HL-60 cells as a model of growth and differentiation: the significance
643 of variant cells. *Hematology Review* 4: 5-46.
- 644 21. Yang T, Xiong Q, Enslen H, Davis R, Chow CW (2002) Phosphorylation of NFATc4
645 by p38 mitogen-activated protein kinases. *Mol Cell Biol* 22: 3892–3904.
- 646 22. Wang J, Yen A (2008) A MAPK-positive Feedback Mechanism for BLR1 Signaling
647 Propels Retinoic Acid-triggered Differentiation and Cell Cycle Arrest. *J Biol Chem*
648 283: 4375–4386.
- 649 23. Geil WM, Yen A (2014) Nuclear raf-1 kinase regulates the cxcr5 promoter by asso-
650 ciating with nfatc3 to drive retinoic acid-induced leukemic cell differentiation. *FEBS*
651 *J* 281: 1170-80.
- 652 24. Tasseff R, Nayak S, Song S, Yen A, Varner J (2011) Modeling and analysis of retinoic
653 acid induced differentiation of uncommitted precursor cells. *Integr Biol* 3: 578 - 591.
- 654 25. Jensen HA, Styskal LE, Tasseff R, Bunaciu RP, Congleton J, et al. (2013) The
655 src-family kinase inhibitor pp2 rescues inducible differentiation events in emergent
656 retinoic acid-resistant myeloblastic leukemia cells. *PLoS One* 8: e58621.
- 657 26. Jensen HA, Bunaciu RP, Ibabao CN, Myers R, Varner JD, et al. (2014) Retinoic acid
658 therapy resistance progresses from unilineage to bilineage in hl-60 leukemic blasts.
659 *PLoS One* 9: e98929.
- 660 27. Jensen HA, Bunaciu RP, Varner JD, Yen A (2015) Gw5074 and pp2 kinase inhibitors
661 implicate nontraditional c-raf and lyn function as drivers of retinoic acid-induced mat-
662 uration. *Cell Signal* 27: 1666-75.
- 663 28. Jensen HA, Yourish HB, Bunaciu RP, Varner JD, Yen A (2015) Induced myelomono-
664 cytic differentiation in leukemia cells is accompanied by noncanonical transcription
665 factor expression. *FEBS Open Bio* 5: 789-800.
- 666 29. Milo R, Jorgensen P, Moran U, Weber G, Springer M (2010) Bionumbers—the
667 database of key numbers in molecular and cell biology. *Nucleic Acids Res* 38: D750-

- 668 3.
- 669 30. Katagiri K, Hattori S, Nakamura S, Yamamoto T, Yoshida T, et al. (1994) Activation
670 of ras and formation of gap complex during tpa-induced monocytic differentiation of
671 hl-60 cells. *Blood* 84: 1780–1789.
- 672 31. Miranda MB, Johnson DE (2007) Signal transduction pathways that contribute to
673 myeloid differentiation. *Leukemia* 21: 1363–1377.
- 674 32. Hickstein DD, Back AL, Collins SJ (1989) Regulation of expression of the cd11b and
675 cd18 subunits of the neutrophil adherence receptor during human myeloid differen-
676 tiation. *J Biol Chem* 264: 21812–21817.
- 677 33. Hornstein I, Alcover A, Katzav S (2004) Vav proteins, masters of the world of cy-
678 toskeleton organization. *Cell Signal* 16: 1-11.
- 679 34. Ferrell J (2002) Self-perpetuating states in signal transduction: positive feedback,
680 double-negative feedback and bistability. *Curr Opin Cell Biol* 14: 140-8.
- 681 35. Laslo P, Spooner CJ, Warmflash A, Lancki DW, Lee HJ, et al. (2006) Multilineage
682 transcriptional priming and determination of alternate hematopoietic cell fates. *Cell*
683 126: 755-66.
- 684 36. Xiong W, Ferrell J (2003) A positive-feedback-based bistable 'memory module' that
685 governs a cell fate decision. *Nature* 426: 460-5.
- 686 37. Bagci EZ, Vodovotz Y, Billiar TR, Ermentrout GB, Bahar I (2006) Bistability in apop-
687 tosis: roles of bax, bcl-2, and mitochondrial permeability transition pores. *Biophys J*
688 90: 1546-59.
- 689 38. Luan D, Zai M, Varner JD (2007) Computationally derived points of fragility of a
690 human cascade are consistent with current therapeutic strategies. *PLoS Comput
691 Biol* 3: e142.
- 692 39. Friedman AD (2007) Transcriptional control of granulocyte and monocyte develop-
693 ment. *Oncogene* 26: 6816-28.

- 694 40. Dahl R, Walsh JC, Lancki D, Laslo P, Iyer SR, et al. (2003) Regulation of macrophage
695 and neutrophil cell fates by the PU.1:C/EBPalpha ratio and granulocyte colony-
696 stimulating factor. *Nat Immunol* 4: 1029-36.
- 697 41. El-Benna J, Dang PMC, Gougerot-Pocidalo MA, Marie JC, Braut-Boucher F (2009)
698 p47phox, the phagocyte nadph oxidase/nox2 organizer: structure, phosphorylation
699 and implication in diseases. *Exp Mol Med* 41: 217-25.
- 700 42. Hock H, Hamblen MJ, Rooke HM, Traver D, Bronson RT, et al. (2003) Intrinsic re-
701 quirement for zinc finger transcription factor gfi-1 in neutrophil differentiation. *Immuni-*
702 *tity* 18: 109-20.
- 703 43. Cleghon V, Morrison DK (1994) Raf-1 interacts with fyn and src in a non-
704 phosphotyrosine-dependent manner. *J Biol Chem* 269: 17749–17755.
- 705 44. Zimmermann S, Moelling K (1999) Phosphorylation and regulation of raf by akt (pro-
706 tein kinase b). *Science* 286: 1741–1744.
- 707 45. Ritt DA, Zhou M, Conrads TP, Veenstra TD, Copeland TD, et al. (2007) Ck2 is a
708 component of the ksr1 scaffold complex that contributes to raf kinase activation.
709 *Curr Biol* 17: 179–184.
- 710 46. Hekman M, Wiese S, Metz R, Albert S, Troppmair J, et al. (2004) Dynamic changes
711 in c-raf phosphorylation and 14-3-3 protein binding in response to growth factor stim-
712 ulation: differential roles of 14-3-3 protein binding sites. *J Biol Chem* 279: 14074–
713 14086.
- 714 47. Dhillon AS, Yip YY, Grindlay GJ, Pakay JL, Dangers M, et al. (2009) The c-terminus
715 of raf-1 acts as a 14-3-3-dependent activation switch. *Cell Signal* 21: 1645–1651.
- 716 48. Song JS, Gomez J, Stancato LF, Rivera J (1996) Association of a p95 vav-containing
717 signaling complex with the fcepsilonlonri gamma chain in the rbl-2h3 mast cell line.
718 evidence for a constitutive in vivo association of vav with grb2, raf-1, and erk2 in an
719 active complex. *J Biol Chem* 271: 26962–26970.

- 720 49. Costello PS, Walters AE, Mee PJ, Turner M, Reynolds LF, et al. (1999) The rho-
721 family gtp exchange factor vav is a critical transducer of t cell receptor signals to the
722 calcium, erk, and nf-kappab pathways. Proc Natl Acad Sci U S A 96: 3035–3040.
- 723 50. Graham D, Robertson C, Bautista J, Mascarenhas F, Diacovo M, et al. (2007)
724 Neutrophil-mediated oxidative burst and host defense are controlled by a Vav-
725 PLCgamma2 signaling axis in mice. J Clin Invest 117: 3445–3452.
- 726 51. Kim HS, Lim IK (2009) Phosphorylated extracellular signal-regulated protein kinases
727 1 and 2 phosphorylate sp1 on serine 59 and regulate cellular senescence via tran-
728 scription of p21sdi1/cip1/waf1. J Biol Chem 284: 15475–15486.
- 729 52. Milanini-Mongiat J, Pouyss?gur J, Pag?s G (2002) Identification of two sp1 phos-
730 phorylation sites for p42/p44 mitogen-activated protein kinases: their implication in
731 vascular endothelial growth factor gene transcription. J Biol Chem 277: 20631–
732 20639.
- 733 53. Zhang Y, Cho YY, Petersen BL, Zhu F, Dong Z (2004) Evidence of stat1 phosphory-
734 lation modulated by mapks, mek1 and msk1. Carcinogenesis 25: 1165–1175.
- 735 54. Li Z, Theus MH, Wei L (2006) Role of erk 1/2 signaling in neuronal differentiation of
736 cultured embryonic stem cells. Dev Growth Differ 48: 513–523.
- 737 55. Yen A, Reece SL, Albright KL (1984) Dependence of hl-60 myeloid cell differentiation
738 on continuous and split retinoic acid exposures: precommitment memory associated
739 with altered nuclear structure. J Cell Physiol 118: 277–286.
- 740 56. Moon TS, Lou C, Tamsir A, Stanton BC, Voigt CA (2012) Genetic programs con-
741 structed from layered logic gates in single cells. Nature 491: 249-53.
- 742 57. Wayman JA, Sagar A, Varner JD (2015) Dynamic modeling of cell-free biochemical
743 networks using effective kinetic models. Processes 3: 138.
- 744 58. Igel C, Hansen N, Roth S (2007) Covariance matrix adaptation for multi-objective
745 optimization. Evol Comput 15: 1-28.

- 746 59. Bezanson J, Edelman A, Karpinski S, Shah VB (2014) Julia: A fresh approach to
747 numerical computing. CoRR abs/1411.1607.
- 748 60. Brooks SC, Kazmer S, Levin AA, Yen A (1996) Myeloid differentiation and retinoblas-
749 toma phosphorylation changes in HL-60 cells induced by retinoic acid receptor- and
750 retinoid X receptor-selective retinoic acid analogs. Blood 87: 227–237.
- 751 61. Rishi AK, Gerald TM, Shao ZM, Li XS, Baumann RG, et al. (1996) Regulation of the
752 human retinoic acid receptor alpha gene in the estrogen receptor negative human
753 breast carcinoma cell lines skbr-3 and mda-mb-435. Cancer Res 56: 5246-52.
- 754 62. Mueller BU, Pabst T, Fos J, Petkovic V, Fey MF, et al. (2006) Atra resolves the dif-
755 ferentiation block in t(15;17) acute myeloid leukemia by restoring pu.1 expression.
756 Blood 107: 3330-8.
- 757 63. Luo XM, Ross AC (2006) Retinoic acid exerts dual regulatory actions on the ex-
758 pression and nuclear localization of interferon regulatory factor-1. Exp Biol Med
759 (Maywood) 231: 619-31.
- 760 64. Sylvester I, Schöler HR (1994) Regulation of the oct-4 gene by nuclear receptors.
761 Nucleic Acids Res 22: 901-11.
- 762 65. Drach J, McQueen T, Engel H, Andreeff M, Robertson KA, et al. (1994) Retinoic
763 acid-induced expression of cd38 antigen in myeloid cells is mediated through
764 retinoic acid receptor-alpha. Cancer Res 54: 1746-52.
- 765 66. Liu M, Iavarone A, Freedman LP (1996) Transcriptional activation of the human
766 p21(waf1/cip1) gene by retinoic acid receptor. correlation with retinoid induction of
767 u937 cell differentiation. J Biol Chem 271: 31723-8.
- 768 67. Bunaciu RP, Yen A (2013) 6-formylindolo (3,2-b)carbazole (ficz) enhances retinoic
769 acid (ra)-induced differentiation of hl-60 myeloblastic leukemia cells. Mol Cancer 12:
770 39.
- 771 68. Balmer JE, Blomhoff R (2002) Gene expression regulation by retinoic acid. J Lipid

- 772 Res 43: 1773-808.
- 773 69. Rosen ED, Hsu CH, Wang X, Sakai S, Freeman MW, et al. (2002) C/ebpalpha in-
- 774 duces adipogenesis through ppargamma: a unified pathway. Genes Dev 16: 22-6.
- 775 70. Varley CL, Bacon EJ, Holder JC, Southgate J (2009) Foxa1 and irf-1 intermediary
- 776 transcriptional regulators of ppargamma-induced urothelial cytodifferentiation. Cell
- 777 Death Differ 16: 103-14.
- 778 71. Bruemmer D, Yin F, Liu J, Berger JP, Sakai T, et al. (2003) Regulation of the growth
- 779 arrest and dna damage-inducible gene 45 (gadd45) by peroxisome proliferator-
- 780 activated receptor gamma in vascular smooth muscle cells. Circ Res 93: e38-47.
- 781 72. Delerive P, De Bosscher K, Besnard S, Vanden Berghe W, Peters JM, et al. (1999)
- 782 Peroxisome proliferator-activated receptor alpha negatively regulates the vascular
- 783 inflammatory gene response by negative cross-talk with transcription factors nf-
- 784 kappaB and ap-1. J Biol Chem 274: 32048-54.
- 785 73. Altiok S, Xu M, Spiegelman BM (1997) Ppargamma induces cell cycle withdrawal:
- 786 inhibition of e2f/dp dna-binding activity via down-regulation of pp2a. Genes Dev 11:
- 787 1987-98.
- 788 74. Fei J, Cook C, Gillespie M, Yu B, Fullen K, et al. (2011) Atherogenic ω -6 lipids mod-
- 789 ulate ppar- egr-1 crosstalk in vascular cells. PPAR Res 2011: 753917.
- 790 75. Song EK, Lee YR, Kim YR, Yeom JH, Yoo CH, et al. (2012) Naadp mediates insulin-
- 791 stimulated glucose uptake and insulin sensitization by ppar γ in adipocytes. Cell Rep
- 792 2: 1607-19.
- 793 76. Szanto A, Nagy L (2005) Retinoids potentiate peroxisome proliferator-activated re-
- 794 ceptor gamma action in differentiation, gene expression, and lipid metabolic pro-
- 795 cesses in developing myeloid cells. Mol Pharmacol 67: 1935-43.
- 796 77. Han S, Sidell N, Fisher PB, Roman J (2004) Up-regulation of p21 gene expres-
- 797 sion by peroxisome proliferator-activated receptor gamma in human lung carcinoma

- 798 cells. Clin Cancer Res 10: 1911-9.
- 799 78. Von Knethen A, Brüne B (2002) Activation of peroxisome proliferator-activated re-
800 ceptor gamma by nitric oxide in monocytes/macrophages down-regulates p47phox
801 and attenuates the respiratory burst. J Immunol 169: 2619-26.
- 802 79. Dispirito JR, Fang B, Wang F, Lazar MA (2013) Pruning of the adipocyte peroxisome
803 proliferator-activated receptor γ cistrome by hematopoietic master regulator pu.1.
804 Mol Cell Biol 33: 3354-64.
- 805 80. Chen H, Ray-Gallet D, Zhang P, Hetherington CJ, Gonzalez DA, et al. (1995) Pu.1
806 (spi-1) autoregulates its expression in myeloid cells. Oncogene 11: 1549-60.
- 807 81. Steidl U, Rosenbauer F, Verhaak RGW, Gu X, Ebralidze A, et al. (2006) Essential
808 role of jun family transcription factors in pu.1 knockdown-induced leukemic stem
809 cells. Nat Genet 38: 1269-77.
- 810 82. Pahl HL, Scheibe RJ, Zhang DE, Chen HM, Galson DL, et al. (1993) The proto-
811 oncogene pu.1 regulates expression of the myeloid-specific cd11b promoter. J Biol
812 Chem 268: 5014-20.
- 813 83. Yuki H, Ueno S, Tatetsu H, Niiro H, Iino T, et al. (2013) Pu.1 is a potent tumor
814 suppressor in classical hodgkin lymphoma cells. Blood 121: 962-70.
- 815 84. Li SL, Schlegel W, Valente AJ, Clark RA (1999) Critical flanking sequences of pu.1
816 binding sites in myeloid-specific promoters. J Biol Chem 274: 32453-60.
- 817 85. Timchenko N, Wilson DR, Taylor LR, Abdelsayed S, Wilde M, et al. (1995) Autoreg-
818 ulation of the human c/ebp alpha gene by stimulation of upstream stimulatory factor
819 binding. Mol Cell Biol 15: 1192-202.
- 820 86. Lidonnici MR, Audia A, Soliera AR, Prisco M, Ferrari-Amorotti G, et al. (2010) Ex-
821 pression of the transcriptional repressor gfi-1 is regulated by c/ebpalpha and is
822 involved in its proliferation and colony formation-inhibitory effects in p210bcr/abl-
823 expressing cells. Cancer Res 70: 7949-59.

- 824 87. D'Alo' F, Johansen LM, Nelson EA, Radomska HS, Evans EK, et al. (2003) The
825 amino terminal and e2f interaction domains are critical for c/ebp alpha-mediated
826 induction of granulopoietic development of hematopoietic cells. *Blood* 102: 3163-
827 71.
- 828 88. Pan Z, Hetherington CJ, Zhang DE (1999) Ccaat/enhancer-binding protein activates
829 the cd14 promoter and mediates transforming growth factor beta signaling in mono-
830 cyte development. *J Biol Chem* 274: 23242-8.
- 831 89. Harris TE, Albrecht JH, Nakanishi M, Darlington GJ (2001) Ccaat/enhancer-binding
832 protein-alpha cooperates with p21 to inhibit cyclin-dependent kinase-2 activity and
833 induces growth arrest independent of dna binding. *J Biol Chem* 276: 29200-9.
- 834 90. Bauvois B, Durant L, Laboureau J, Barthélémy E, Rouillard D, et al. (1999) Upreg-
835 ulation of cd38 gene expression in leukemic b cells by interferon types i and ii. *J*
836 *Interferon Cytokine Res* 19: 1059-66.
- 837 91. Passioura T, Dolnikov A, Shen S, Symonds G (2005) N-ras-induced growth suppres-
838 sion of myeloid cells is mediated by irf-1. *Cancer Res* 65: 797-804.
- 839 92. Dahl R, Iyer SR, Owens KS, Cuylear DD, Simon MC (2007) The transcriptional
840 repressor gfi-1 antagonizes pu.1 activity through protein-protein interaction. *J Biol*
841 *Chem* 282: 6473-83.
- 842 93. Duan Z, Horwitz M (2003) Targets of the transcriptional repressor oncoprotein gfi-1.
843 *Proc Natl Acad Sci U S A* 100: 5932-7.
- 844 94. Chen H, Zhang P, Radomska HS, Hetherington CJ, Zhang DE, et al. (1996) Octamer
845 binding factors and their coactivator can activate the murine pu.1 (spi-1) promoter.
846 *J Biol Chem* 271: 15743-52.
- 847 95. Behre G, Whitmarsh AJ, Coghlan MP, Hoang T, Carpenter CL, et al. (1999) c-jun
848 is a jnk-independent coactivator of the pu.1 transcription factor. *J Biol Chem* 274:
849 4939-46.

- 850 96. Kardassis D, Papakosta P, Pardali K, Moustakas A (1999) c-jun transactivates the
851 promoter of the human p21(waf1/cip1) gene by acting as a superactivator of the
852 ubiquitous transcription factor sp1. *J Biol Chem* 274: 29572-81.
- 853 97. Johnson DG, Ohtani K, Nevins JR (1994) Autoregulatory control of e2f1 expression
854 in response to positive and negative regulators of cell cycle progression. *Genes Dev*
855 8: 1514-25.
- 856 98. Fu M, Zhang J, Lin Y, Zhu X, Ehrengruber MU, et al. (2002) Early growth response
857 factor-1 is a critical transcriptional mediator of peroxisome proliferator-activated
858 receptor-gamma 1 gene expression in human aortic smooth muscle cells. *J Biol
859 Chem* 277: 26808-14.
- 860 99. Mak KS, Funnell APW, Pearson RCM, Crossley M (2011) Pu.1 and haematopoietic
861 cell fate: Dosage matters. *Int J Cell Biol* 2011: 808524.
- 862 100. Chen F, Wang Q, Wang X, Studzinski GP (2004) Up-regulation of egr1 by 1,25-
863 dihydroxyvitamin d3 contributes to increased expression of p35 activator of cyclin-
864 dependent kinase 5 and consequent onset of the terminal phase of hl60 cell differ-
865 entiation. *Cancer Res* 64: 5425-33.
- 866 101. Suh J, Jeon YJ, Kim HM, Kang JS, Kaminski NE, et al. (2002) Aryl hydrocarbon
867 receptor-dependent inhibition of ap-1 activity by 2,3,7,8-tetrachlorodibenzo-p-dioxin
868 in activated b cells. *Toxicol Appl Pharmacol* 181: 116-23.
- 869 102. Shen M, Bunaciu RP, Congleton J, Jensen HA, Sayam LG, et al. (2011) Inter-
870 feron regulatory factor-1 binds c-cbl, enhances mitogen activated protein kinase
871 signaling and promotes retinoic acid-induced differentiation of hl-60 human myelo-
872 monoblastic leukemia cells. *Leuk Lymphoma* 52: 2372-9.
- 873 103. Bunaciu RP, Yen A (2011) Activation of the aryl hydrocarbon receptor ahr promotes
874 retinoic acid-induced differentiation of myeloblastic leukemia cells by restricting ex-
875 pression of the stem cell transcription factor oct4. *Cancer Res* 71: 2371-80.

- 876 104. Jackson DA, Pombo A, Iborra F (2000) The balance sheet for transcription: an anal-
877 ysis of nuclear rna metabolism in mammalian cells. *FASEB J* 14: 242-54.
- 878 105. Zhao ZW, Roy R, Gebhardt JCM, Suter DM, Chapman AR, et al. (2014) Spatial orga-
879 nization of rna polymerase ii inside a mammalian cell nucleus revealed by reflected
880 light-sheet superresolution microscopy. *Proc Natl Acad Sci U S A* 111: 681-6.
- 881 106. Freitas R, Merkle R (2004) Kinematic Self-Replicating Machines. Oxford University
882 Press.
- 883 107. Yang E, van Nimwegen E, Zavolan M, Rajewsky N, Schroeder M, et al. (2003) De-
884 cay rates of human mrnas: correlation with functional characteristics and sequence
885 attributes. *Genome Res* 13: 1863-72.
- 886 108. Doherty MK, Hammond DE, Clague MJ, Gaskell SJ, Beynon RJ (2009) Turnover
887 of the human proteome: determination of protein intracellular stability by dynamic
888 silac. *J Proteome Res* 8: 104-12.
- 889 109. Sehgal PB, Derman E, Molloy GR, Tamm I, Darnell JE (1976) 5,6-dichloro-1-beta-
890 d-ribofuranosylbenzimidazole inhibits initiation of nuclear heterogeneous rna chains
891 in hela cells. *Science* 194: 431-3.
- 892 110. Darzacq X, Shav-Tal Y, de Turris V, Brody Y, Shenoy SM, et al. (2007) In vivo dy-
893 namics of rna polymerase ii transcription. *Nat Struct Mol Biol* 14: 796-806.
- 894 111. Kos M, Tollervey D (2010) Yeast pre-rrna processing and modification occur cotran-
895 scriptionally. *Mol Cell* 37: 809-20.
- 896 112. Darnell JE Jr (2013) Reflections on the history of pre-mrna processing and highlights
897 of current knowledge: a unified picture. *RNA* 19: 443-60.
- 898 113. Boström K, Wettsten M, Borén J, Bondjers G, Wiklund O, et al. (1986) Pulse-chase
899 studies of the synthesis and intracellular transport of apolipoprotein b-100 in hep g2
900 cells. *J Biol Chem* 261: 13800-6.
- 901 114. Meyers R, editor (2004) Encyclopedia of Molecular Cell Biology and Molecular

- 902 Medicine, Volume 1, 2nd Edition. ISBN: 978-3-527-30543-8. Wiley-Blackwell.
- 903 115. Rosenbluth MJ, Lam WA, Fletcher DA (2006) Force microscopy of nonadherent
- 904 cells: a comparison of leukemia cell deformability. *Biophys J* 90: 2994-3003.
- 905 116. O'Leary NA, Wright MW, Brister JR, Ciufo S, Haddad D, et al. (2016) Reference
- 906 sequence (refseq) database at ncbi: current status, taxonomic expansion, and func-
- 907 tional annotation. *Nucleic Acids Res* 44: D733-45.

Table 1: Myelomonocytic transcription factor connectivity used in the signal integration and phenotype modules.

Effector	Effect	Target	Source
RAR α	+	RAR α	(61)
	+	PU.1	(62)
	+	C/EBP α	(39)
	+	IRF-1	(63)
	-	Oct4	(64)
	+	CD38	(65)
	+	p21	(66)
	+	AhR	(67)
	+	Egr-1	(68)
PPAR γ	+	C/EBP α	(69)
	+	IRF-1	(70)
	+	Oct1	(71)
	-	AP-1	(72)
	-	E2F	(73)
	-	Egr-1	(74)
	+	CD38	(75)
	+	CD14	(76)
	+	p21	(77)
	-	p47Phox	(78)
PU.1	-	PPAR γ	(79)
	+	PU.1	(80)
	+	AP-1	(81)
	+	Egr-1	(35)
	+	CD11b	(82)
	+	p21	(83)
	+	p47Phox	(84)
C/EBP α	+	PPAR γ	(69)
	+	PU.1	(40)
	+	C/EBP α	(85)
	+	Gfi-1	(86)
	-	E2F	(87)
	+	CD14	(88)

909

	+	p21	(89)
IRF-1	+	CD38	(90)
	+	p21	(91)
	-	PU.1	(92)
	-	C/EBP α	(93)
	-	E2F	(93)
	-	Egr-1	(35)
	-	p21	(93)
Oct1	+	PU.1	(94)
AP-1	-	PPAR γ	(72)
	+	PU.1	(95)
	+	p21	(96)
E2F	+	E2F	(97)
Egr-1	+	PPAR γ	(98)
	-	Gfi-1	(99)
	+	CD14	(100)
AhR	+	AP-1	(101)
	+	IRF-1	(102)
	-	Oct4	(103)
	-	PU.1	

Table 2: Characteristic model parameters estimated from literature.

Symbol	Description	Value	Units	Source
R_1	RNA polymerase abundance	85,000	copies/cell	(104, 105)
R_2	Ribosome abundance	1×10^6	copies/cell	(106)
G_i	Characteristic gene abundance	2	copies/cell	this study
K_X	Saturation constant transcription	600	copies/cell	this study
K_T	Saturation constant translation	95,000	copies/cell	this study
$t_{1/2,m}$	characteristic mRNA half-life (transcription factor)	2-4	hr	(107)
$t_{1/2,p}$	characteristic protein half-life	10	hr	(108)
$\theta_{m,j}$	characteristic mRNA degradation constant	0.34	hr^{-1}	derived
$\theta_{p,j}$	characteristic protein degradation constant	0.07	hr^{-1}	derived
912	t_d	HL-60 doubling time	19.5	hr
	μ	growth rate	0.035	hr^{-1}
	k_d	death rate	0.10μ	hr^{-1}
	e_T	elongation rate RNA polymerase	50-100	nt/s
	e_X	elongation rate Ribosome	5	aa/s
	$L_{T,o}$	characteristic gene length	15,000	nt
	$L_{X,o}$	characteristic transcript length	5,000	nt
	k_T	characteristic transcription rate	1.44	hr^{-1}
	k_X	characteristic translation rate	3.60	hr^{-1}
	D	Diameter of an HL-60 cell	12.4	μm^3
	f_C	cytoplasmic fraction	0.51	dimensionless

913 **Table 3:** Sequence lengths from NCBI RefSeq database was used in the signal integration and phenotype
 914 modules (116). The RNA sequence length used represents the total distance of transcription, and assume
 to be equal to the gene length.

Gene Name	Gene (bp)	RNA (bp)	Protein (AA)	Gene ID	Protein ID
AP-1	10323	10323	331	Gene ID: 3725	NP_002219
AhR	47530	47530	848	Gene ID: 196	NP_001621
CD11b	72925	72925	1153	Gene ID: 3684	NP_001139280
CD14	8974	8974	375	Gene ID: 929	NP_001035110
CD38	174978	74978	300	Gene ID: 952	NP_001766
C/EBP α	2630	2630	393	Gene ID: 1050	NP_001274353.1
E2F	17919	17919	437	Gene ID: 1869	NP_005216
Egr-1	10824	10824	543	Gene ID: 1958	NP_001955
Gfi-1	13833	13833	422	Gene ID: 2672	NP_005254
IRF-1	16165	16165	325	Gene ID: 3659	NP_002189
Oct1	206516	206516	741.33	Gene ID: 5451	NP_002688.3, NP_001185712.1, NP_001185715.1
Oct4	6356	6356	206.33	Gene ID: 5460	NP_001167002, NP_001167015, NP_001167016
P21	15651	15651	198	NG_009364.1	NP_001621
P47	3074	3074	390	GenBank: AF003533.1	NP_000256
PPAR γ	153507	153507	250	Gene ID: 5468	NP_001317544
PU.1	40782	40782	270.5	Gene ID: 6688	NP_001074016, NP_003111

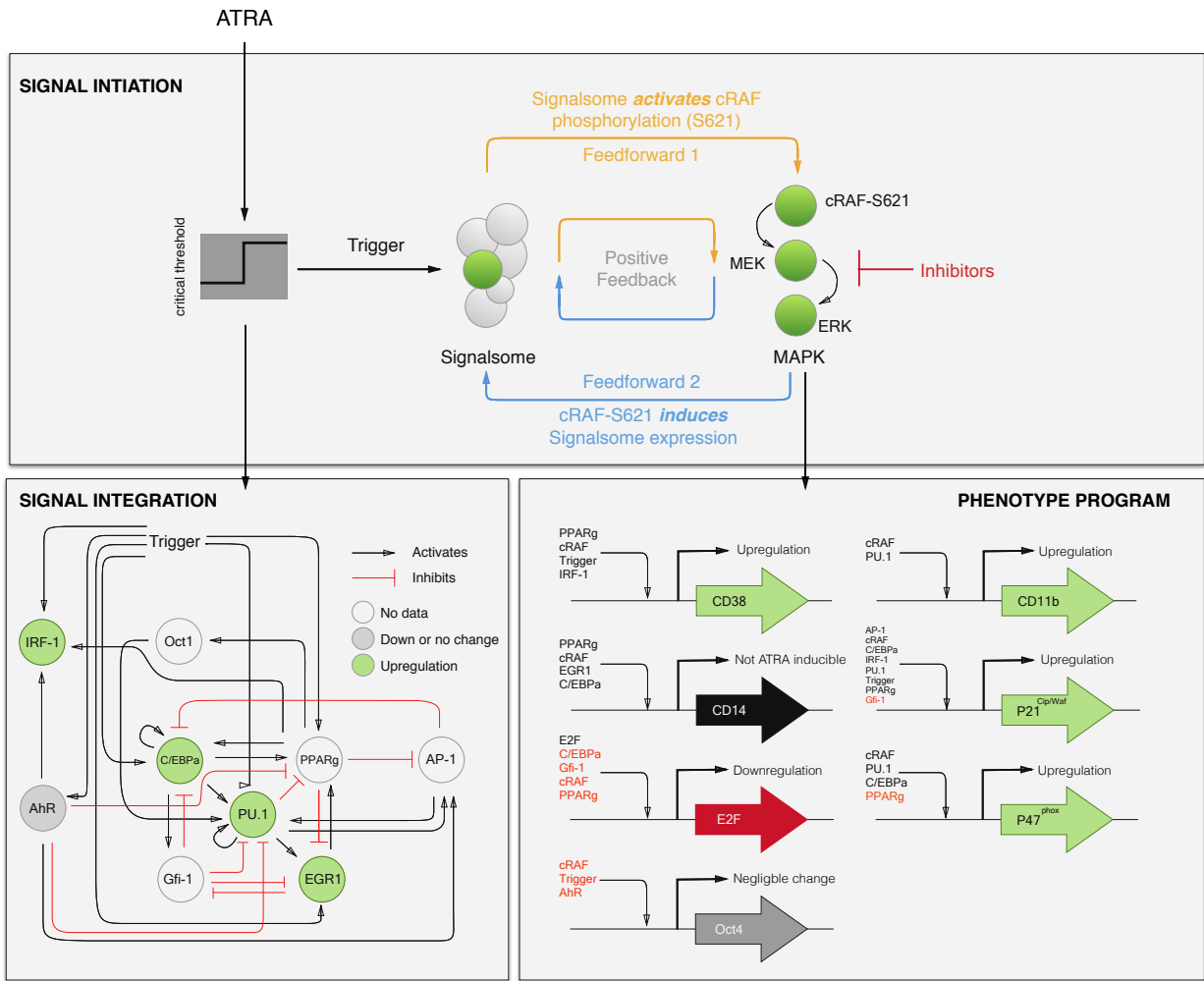


Fig. 1: Schematic of the effective ATRA differentiation circuit. Above a critical threshold, ATRA activates an upstream Trigger, which induces signalsome complex formation. Signalsome activates the mitogen-activated protein kinase (MAPK) cascade which in turn drives the differentiation program and signalsome formation. Both Trigger and activated cRaf-pS621 drive a phenotype gene expression program responsible for differentiation. Trigger activates the expression of a series of transcription factors which in combination with cRaf-pS621 result in phenotypic change.

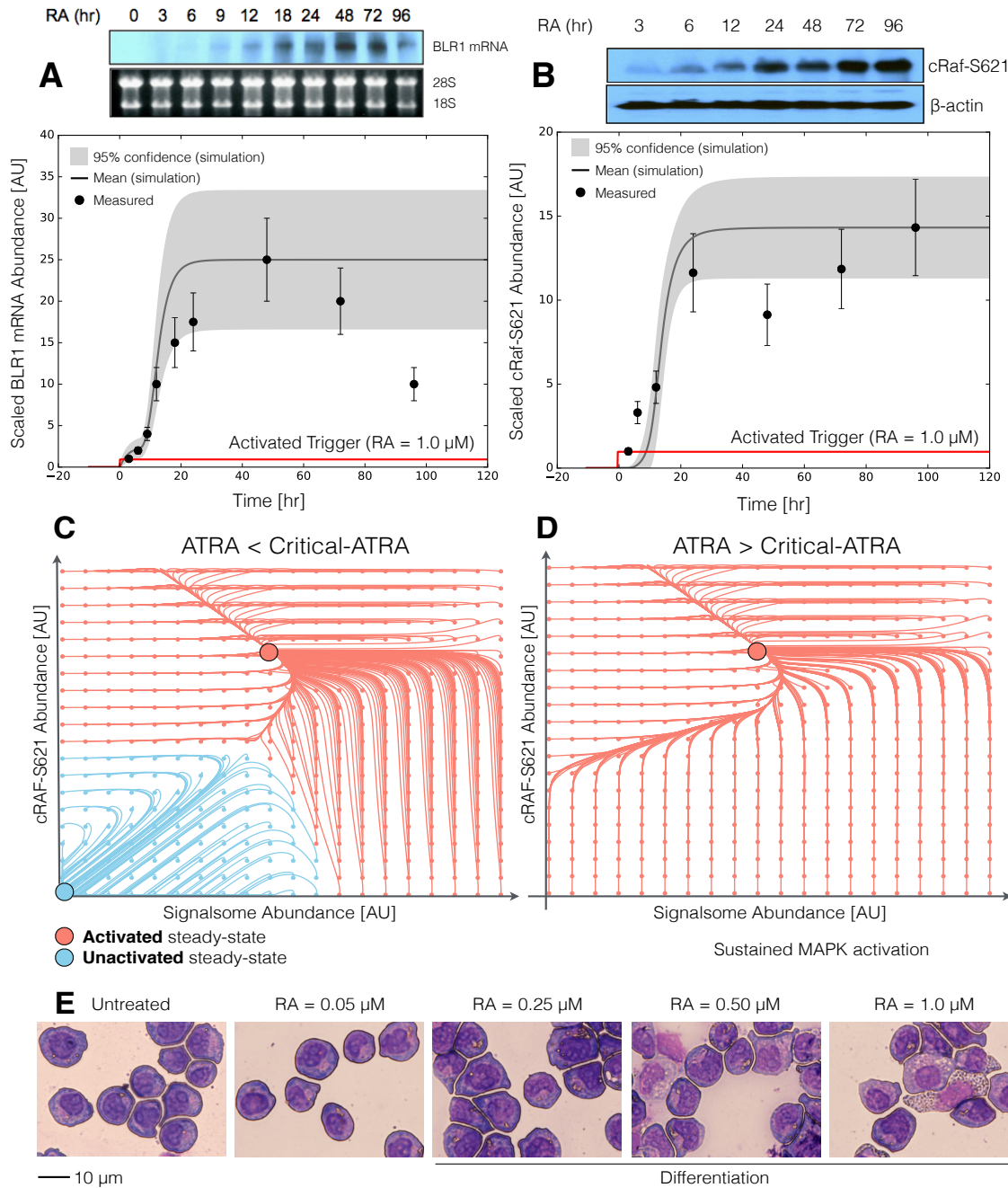


Fig. 2: Model analysis for ATRA-induced HL-60 differentiation. A: BLR1 mRNA versus time following exposure to 1 μ M ATRA at t = 0 hr. B: cRaf-pS621 versus time following exposure to 1 μ M ATRA at t = 0 hr. Points denote experimental measurements, solid lines denote the mean model performance. Shaded regions denote the 99% confidence interval calculated over the parameter ensemble. C: Signalsome and cRaf-pS621 nullclines for ATRA below the critical threshold. The model had two stable steady states and a single unstable state in this regime. D: Signalsome and cRaf-pS621 nullclines for ATRA above the critical threshold. In this regime the model had only a single stable steady state. E: Morphology of HL-60 as a function of ATRA concentration (t = 72 hr).

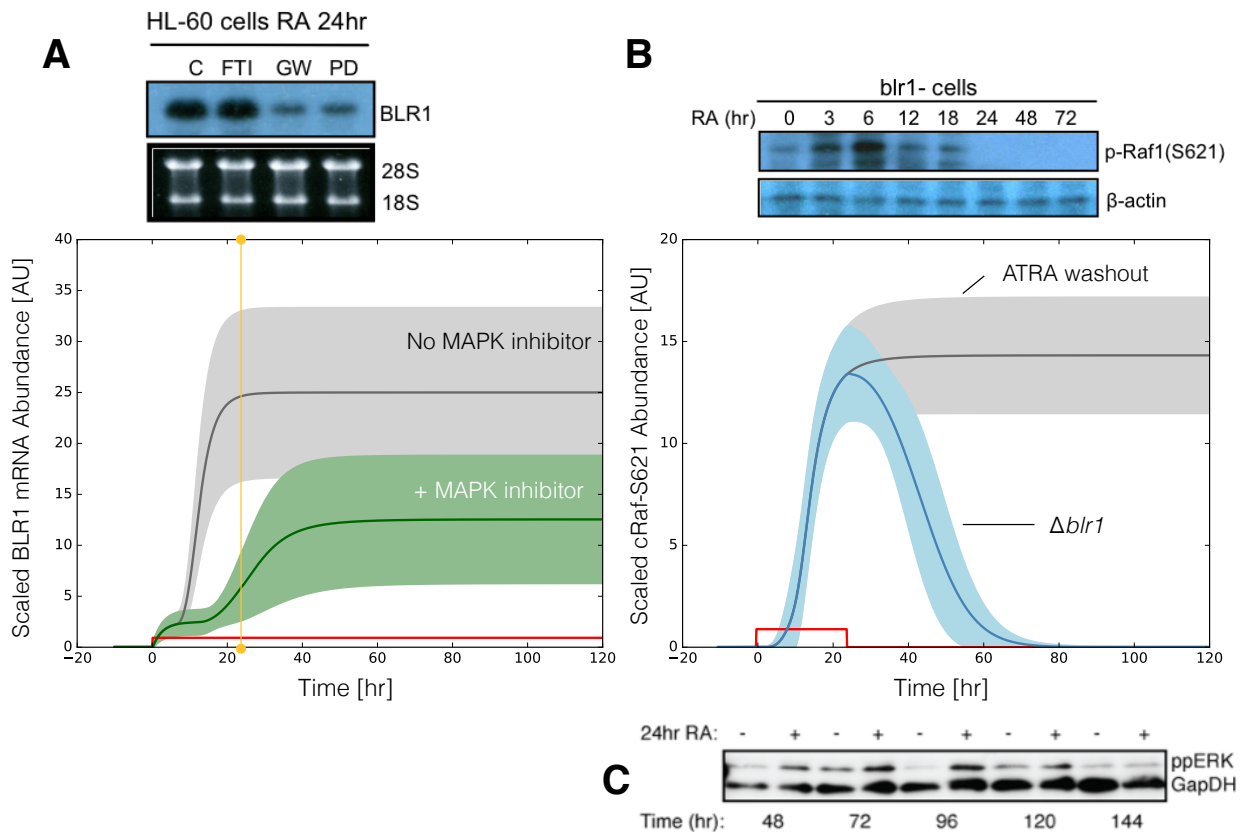


Fig. 3: Model simulation following exposure to $1\mu\text{M}$ ATRA. A: BLR1 mRNA versus time with and without MAPK inhibitor. B: cRaf-pS621 versus time following pulsed exposure to $1\mu\text{M}$ ATRA with and without BLR1. Solid lines denote the mean model performance, while shaded regions denote the 99% confidence interval calculated over the parameter ensemble. C: Western blot analysis of phosphorylated ERK1/2 in ATRA washout experiments. Experimental data in panels A and B were reproduced from Wang and Yen (22), data in panel C is reported in this study.

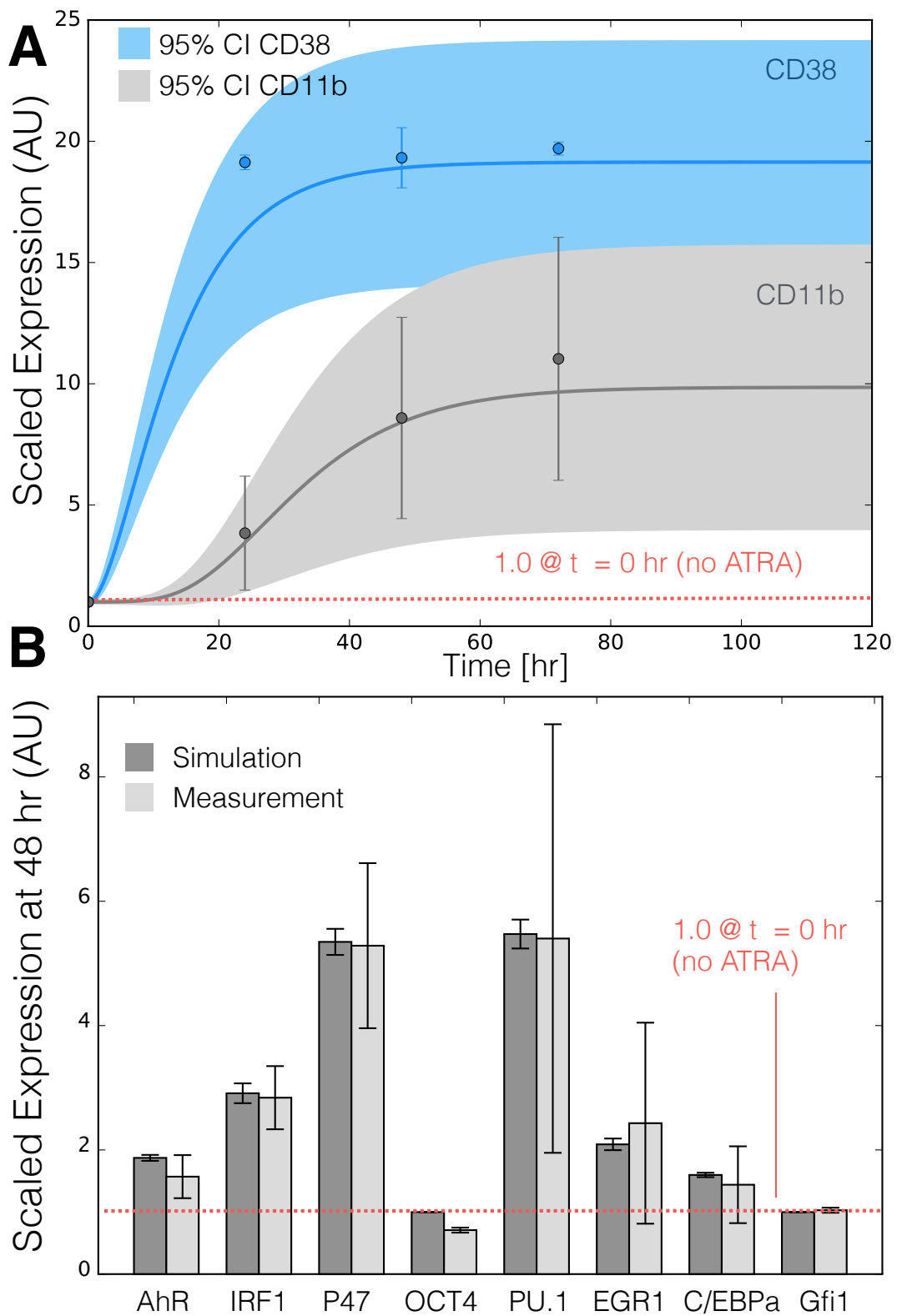


Fig. 4: Model simulation of the HL-60 gene expression program following exposure to $1\mu\text{M}$ ATRA at $t = 0$ hr. A: CD38 and CD11b expression versus time following ATRA exposure at time $t = 0$ hr. B: Gene expression at $t = 48$ hr following ATRA exposure. Experimental data in panels A and B were reproduced from Jensen et al. (28).

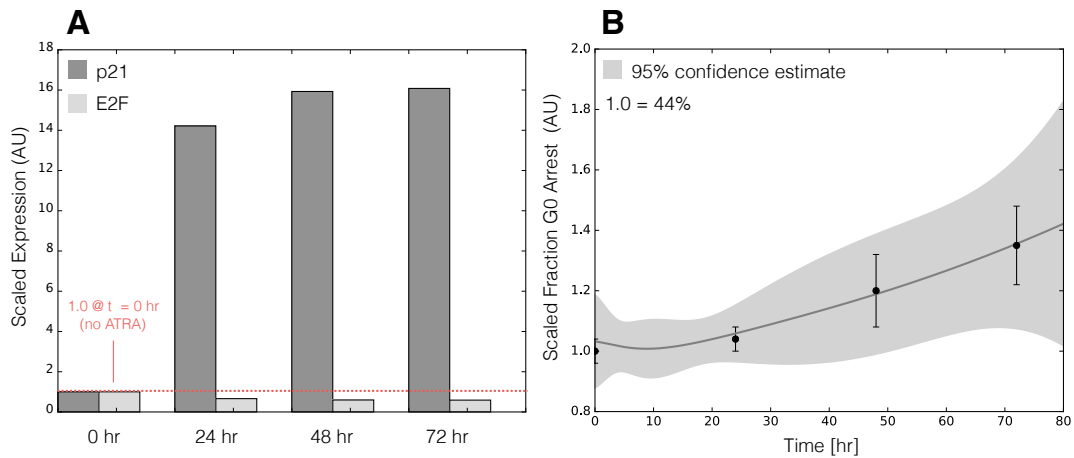


Fig. 5: Model simulation of HL-60 cell-cycle arrest following exposure to $1\mu\text{M}$ ATRA at $t = 0$ hr. A: Predicted p21 and E2F expression levels for the best parameter set following ATRA exposure at time $t = 0$ hr. B: Estimated fraction of HL-60 cells in G0 arrest following ATRA exposure at time $t = 0$ hr. The gray region denotes the 95% confidence estimate of the polynomial model. Experimental data in panel B was reproduced from Jensen et al. (28).

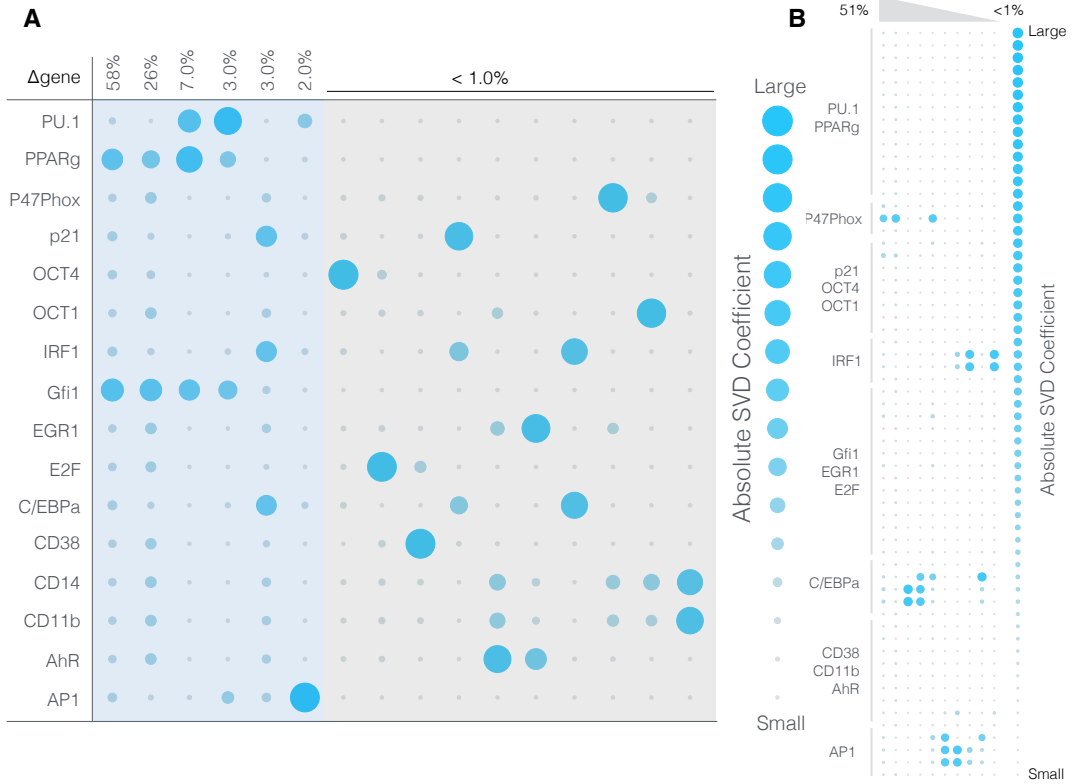


Fig. 6: Robustness of the HL-60 differentiation program following exposure to $1\mu\text{M}$ ATRA at $t = 0$ hr. A: Singular value decomposition of the system response (l^2 -norm between the perturbed and nominal state) following pairwise gene knockout simulations using the best fit parameter set. The percentage at the top of each column describes the fraction of the variance in the system state captured by the node combinations in the rows. B: Singular value decomposition of the system response (l^2 -norm between the perturbed and nominal state) following the pairwise removal of connections.

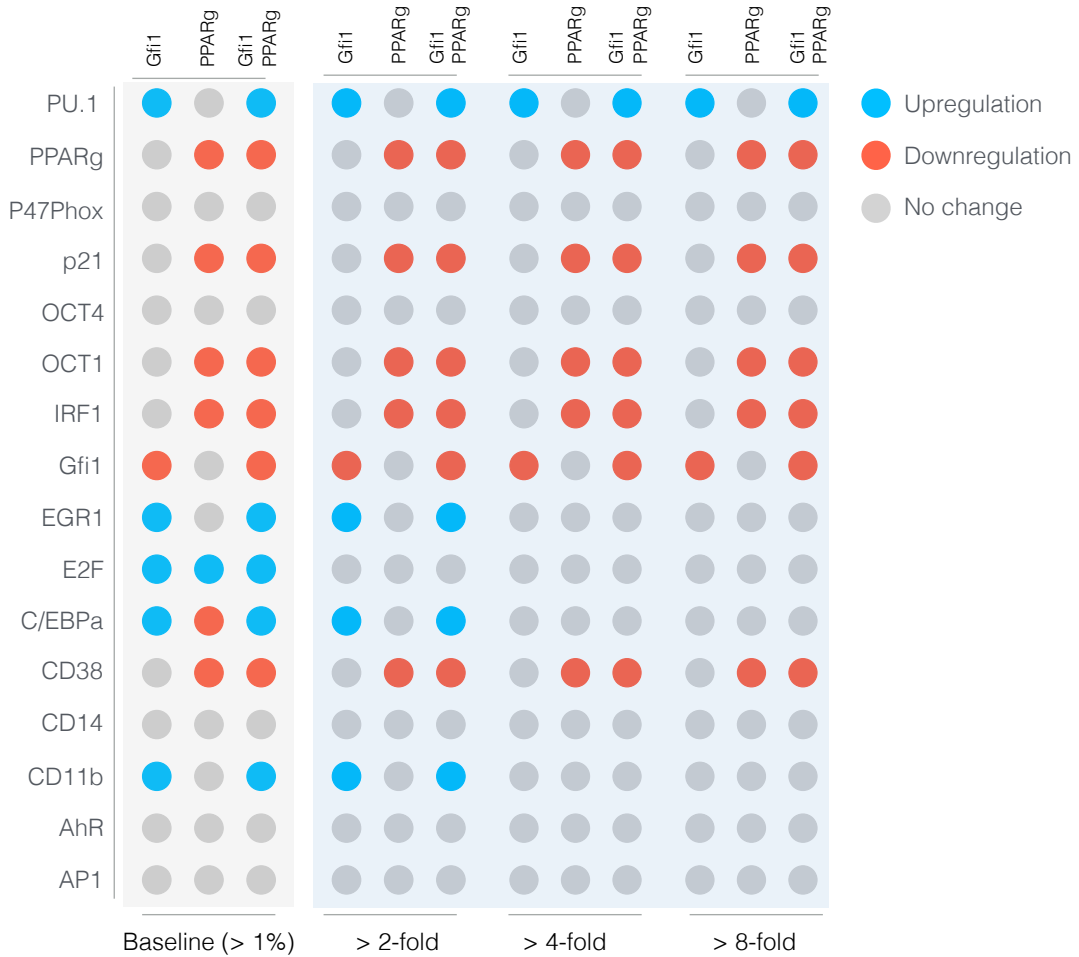


Fig. 7: Robustness of the HL-60 differentiation program following exposure to $1\mu\text{M}$ ATRA at $t = 0$ hr. Protein fold change at $t = 48$ hr (rows) in single and double knock-out mutants (columns) relative to wild-type HL-60 cells. The responses were grouped into $>2,4$ and 8 fold changes. The best fit parameter set was used to calculate the protein fold change.

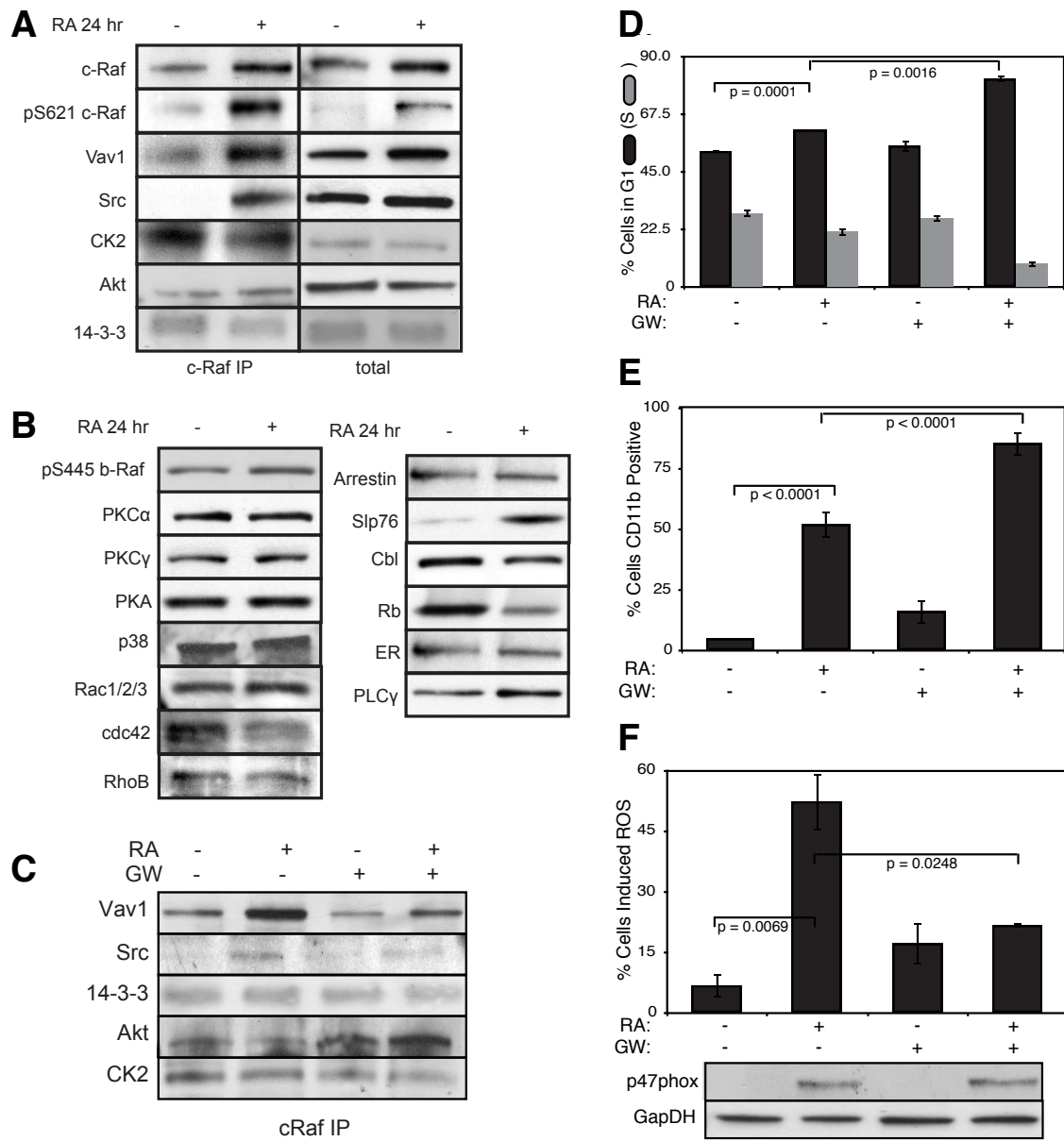


Fig. 8: Investigation of a panel of possible Raf interaction partners in the presence and absence of ATRA. A: Species identified to precipitate out with Raf: first column shows Western blot analysis on total Raf immunoprecipitation with and without 24 hr ATRA treatment and the second on total lysate. B: The expression of species considered that did not precipitate out with Raf at levels detectable by Western blot analysis on total lysate. C: Effect of the Raf inhibitor GW5074 on Raf interactions as determined by Western blot analysis of total Raf immunoprecipitation. The Authors note the signal associated with Src was found to be weak. D: Cell Cycle distribution as determined by flow cytometry indicated arrest induced by ATRA, which was increased by the addition of GW5074. E: Expression of the cell surface marker CD11b as determined by flow cytometry indicated increased expression induced by ATRA, which was enhanced by the addition of GW5074. F: Inducible reactive oxygen species (ROS) as determined by DCF flow cytometry. The functional differentiation response of ATRA treated cells was mitigated by GW5074.